

## 1 **High-Throughput Optimization of Paper-Based Cell-Free Biosensors**

2 David C. Garcia<sup>1</sup>, John P. Davies<sup>1</sup>, Charles E. Davidson<sup>2</sup>, Daniel A. Phillips<sup>1</sup>, Aleksandr E.  
3 Miklos<sup>1</sup>, Matthew W. Lux<sup>1\*</sup>

4 <sup>1</sup>US Army DEVCOM Chemical Biological Center, Aberdeen Proving Ground, MD, USA

5 <sup>2</sup>Science and Technology Corporation, Belcamp, MD, USA

### 6 **Abstract**

7 Cell-free expression systems maintain core cellular processes without intact cells and offer  
8 attractive properties as point-of-need biosensors. The ability to lyophilize, store, and use on-  
9 demand make these sensors usable in the field, and the lack of membranes means that there  
10 are no analyte transport issues and that new sensors can be deployed by simply adding a  
11 different DNA molecule. The lack of membranes also means that sensor designs and reaction  
12 optimizations can be screened in high throughput. While shelf stability has been demonstrated  
13 in specific cases using additives, these approaches are not universal to the myriad cell-free  
14 expression methods and formats. Here, we present new high-throughput screening methods to  
15 optimize cell-free expression formulations when embedded into paper for use as sensors. Our  
16 method leverages acoustic liquid handling to dispense reactions onto 384-well paper ticket  
17 formats and machine vision to quantify reaction performance from a colorimetric reporter  
18 enzyme. The throughput enabled shifts the bottleneck from experimental execution to selecting  
19 the experiments to execute; we therefore implement design-of-experiments to optimize the  
20 information gained from each design-build-test-learn cycle. We used these approaches to first  
21 optimize the performance of a low-cost cell-free expression formulation that was initially non-  
22 functional when embedded in paper, then further optimize it for tolerance to exposure to heat.  
23 With only 2 rounds of experimentation lasting 4 days total for each goal, the result are an energy  
24 mixture with 8% of the materials cost of a commonly used version and a formulation of  
25 excipients that maintain 60% of activity after 6 hours of storage at 50 °C and. Finally, we

26 showcase the use of the cost-optimized formulation in a 3D-printed paperfluidic device where it  
27 outperforms the standard formulation at much lower cost.

## 28 **Keywords**

29 Cell-free expression; synthetic biology; biosensors; paper-based sensors; shelf-stability; design  
30 of experiments

31 Synthetic biology's increasing use of large datasets has significantly improved the process of  
32 repurposing and reengineering natural biological systems towards addressing global  
33 challenges. For instance, rewiring molecular biosensors and their associated genetic networks  
34 have resulted in simple-to-use and cheap biological diagnostics capable of responding to  
35 environmental perturbations dangerous to human health. The use of cell-free expression (CFE)  
36 systems enables gene expression from non-living, *in vitro* biochemical reactions powered by  
37 lysed cells and/or purified transcription and translation components combined with mixtures of  
38 function-encoding nucleic acids, cofactors, and energy sources<sup>1,2</sup>. Biological sensors developed  
39 from these CFE systems have led to a multipurpose platform capable of sensing a variety of  
40 analytes including: pathogen biomarkers, environmental contaminants, and industrial precursors  
41 and products<sup>3-8</sup>.

42 Extending the capability of cell-free biosensors requires that they can effectively be produced,  
43 stored, and used in austere and resource-limited environments<sup>11</sup>. The ability to freeze-dry and  
44 embed cell-free biological components into matrices promises to enable their field-  
45 deployability<sup>9,10</sup>. Cell-free paper sensors address fieldability needs as they can be easy to read  
46 without external devices when paired with visual reporters, are small and disposable, and can  
47 be adapted to different applications by changing the DNA encoding the sensor functionality<sup>12</sup>.  
48 However, cell-free sensors can be rendered ineffective due to non-ideal conditions such as  
49 breaks in cold-chain and reduced access to relevant components<sup>13</sup>. Previous efforts have

50 demonstrated methods involving cryoprotectants that enable shelf stability of CFE reactions for  
51 months at room temperature and 37°C in non-paper formats<sup>14–16</sup>; one early study showed ~20%  
52 activity after 1 year of storage of CFE reactions on paper without cryoprotectants<sup>4</sup>. The cost of  
53 CFE reactions is also an important factor for the technology to reach its potential. While several  
54 studies have assessed materials costs, one formulation offers substantially lower cost while  
55 maintaining substantial yield<sup>17</sup>; until recently, to our knowledge no further published efforts had  
56 taken advantage of this formulation, and still none have tested it for biological sensors. Beyond  
57 cost, disruptions to supply lines due to the COVID19 pandemic impacted the cell-free  
58 community as critical components, especially tRNAs, became increasingly scarce to the point of  
59 near absence from traditional marketplaces<sup>18,19</sup>. As a result, developing a low-cost CFE  
60 formulation that works well on paper and is more resilient to supply chain disruptions would  
61 have a substantial impact on the viability of CFE sensors for a range of applications.

62

63 Addressing this need benefits from the use of high-throughput testing platforms and  
64 methodologies capable of significantly reducing the timeframe for design-build-test-learn (DBTL)  
65 cycles<sup>20</sup>. Previous work using high-throughput methods for aqueous reactions have been shown  
66 to effectively improve CFE performance for new organisms, metabolic reactions, and general  
67 CFE reaction dynamics<sup>21–23</sup>. None of these methods have been applied to sensors or reactions  
68 involving solid matrices like paper; instead, paper sensors have been tested using time- and  
69 labor-intensive methodologies, limiting their use as a testing platform. To alleviate this  
70 bottleneck, we developed a high-throughput testing platform specifically for reactions on paper  
71 and implemented a design-of-experiments (DOE) approach to take advantage of the  
72 throughput. DOE allows for systematic exploration and optimization of complex systems by  
73 elucidating factors with a significant effect on a desired response; this allows experimenters to  
74 determine optimum formulations in a complex system using a fraction of the number of  
75 experiments compared to testing one factor at a time or even some machine learning

76 methodologies<sup>20,23–25</sup>. We applied these methods to optimize a low-cost CFE system that was  
77 originally inactive on paper to perform on par with standard systems, then optimized additives to  
78 improve the stability of CFE sensors to storage at elevated temperatures. With only 2 rounds of  
79 experimentation, one exploratory and one predictive, our efforts led to cell-free paper ticket  
80 sensors that maintained performance at 8% of the original cost as well as formulations capable  
81 of functioning following exposure to 50 °C temperatures for 6 hours. Further, the decreased-cost  
82 mixture was found to be more effective than standard mixtures when used in a 3D-printed  
83 paperfluidic device.

## 84 **Materials and Methods**

### 85 *384-well Ticket Preparation*

86 Wax tickets were printed directly on 1CHR chromatography paper (Whatman) using a Xerox  
87 ColorQube printer and prepared for use in the following manner: each ticket was baked at 125  
88 °C for 5 minutes, allowed to cool at room temperature for 5 min, incubated for 1 h in 5% BSA,  
89 washed thrice with diH<sub>2</sub>O, and allowed to dry overnight in a fume hood. Paper tickets were  
90 stored in fume hood until use.

### 91 *Preparing and Running Cell-Free Reactions*

92 All CFE reactions utilized either a pY71 plasmid with a T7-expressed LacZ insert (pY71-LacZ)  
93 or a combination of two plasmids using the pUCGA vector, one for T7-expression of trH RNA  
94 and the other for T7-expression of swH-lacZ RNA. All DNA was ordered from Aldevron as Giga  
95 Preps.

## 96 *T7 Polymerase Expression Protocol*

97 An overnight culture of cells was grown in LB Media with Ampicillin at 37 °C. The next day 500  
98 mL of LB was inoculated with 1 mL of the overnight culture and grown at 37 °C until the OD600  
99 reached 0.4. Protein expression was induced by adding IPTG to a final concentration of 100 µM,  
100 and the culture was incubated overnight at 37°C. The cells were then pelleted at 5,000 g for 20  
101 minutes at 4 °C and resuspended in 25 mL lysis buffer (1/2x PBS, 0.01% Triton X-100, 1 mM  
102 EDTA). The cells were lysed by sonication, and the lysate was centrifuged to pellet the cellular  
103 debris at 30,000 g for 30 minutes at 4 °C. The supernatant was then transferred to a clean 50  
104 mL tube, with 1.0 mL of Ni-NTA purification resin and incubated for 1 hour at 4 °C with shaking.  
105 We used 20 mL of wash buffer to clean the resin (50 mM phosphate, 300 mM NaCl, 10 mM  
106 imidazole, pH 7.5) and eluted using a gravity flow (50 mM phosphate, 300 mM NaCl, 250 mM  
107 imidazole, pH 7.5). Protein-containing fractions were combined and dialyzed in a 3.5k MWCO  
108 dialysis cassette against 2L of S30 buffer overnight at 4°C and subsequently at -20 °C.

## 109 *E. coli Lysate Preparation*

110 Lysate preparation was carried out using *E. coli* Rosetta (DE3)  $\Delta$ lacZ strains for all experiments.  
111 A 100L culture of Rosetta (DE3)  $\Delta$ lacZ cells was processed for lysate production similar to the  
112 previously described production of BL21(DE3)\* lysate, but with modifications to accommodate  
113 production at scale. Briefly, 750 mL starter cultures (1.5 L total) were grown for 16 hours at 37°C  
114 with 200 rpm shaking incubation. Prior to inoculation, 100 L of 2X YT+P culture media  
115 supplemented with 5 mL of antifoam 204 (Sigma, A8311) in an IF 150L (New Brunswick  
116 Scientific) fermenter was allowed to aerate overnight with a rotor speed of 100 rpm and 20  
117 standard liters per minute (slpm) airflow at 37°C. Following inoculation to a starting OD600 of  
118 0.05, the fermenter settings were adjusted to 300 rpm, 50 splm, and the dissolved oxygen (DO)  
119 was calibrated to 100%. Upon reaching an OD600 of 0.6-1.0, the culture was induced with a

120 final concentration of 1 mM isopropyl B-D-1-thiogalactopyranoside (IPTG) (GoldBio, I2481C).  
121 Once DO reached 50%, the rotor speed was increased to 500 rpm. At an OD600 of 3.5, the  
122 culture was cooled to 4°C, centrifuged in a prechilled Powerfuge pilot, 1.1 L bowl system (CARR  
123 Biosystems) within approximately 8 hours, and the pelleted bacteria was subsequently  
124 processed as described previously.

### 125 *Preparing and Running Cell-Free Reactions*

126 All CFE reactions utilized either a pY71 plasmid with a T7-expressed LacZ insert (pY71-LacZ)  
127 or a combination of two plasmids using the pUCGA vector, one for T7-expression of trH RNA  
128 and the other for T7-expression of swH-lacZ RNA. All DNA was ordered from Aldevron as Giga  
129 Preps. CFE reactions contained 30% v/v lysate and PANOX-sp or Cai buffer as described in  
130 detail previously<sup>25</sup>. All components and final concentrations are summarized in Table S1-3. After  
131 mixing, CFPS reactions were lyophilized in plates, tubes, or vials depending on the scale  
132 described for specific experiments. Base CFE reactions were modified with excipients and  
133 reagents using working solutions based on each experiment and distributed by Echo liquid  
134 handler; PANOX-SP, Cai energy mixture, and excipient working solutions found in **(Tables S4-**  
135 **5)**. Amounts of additional reagents for the optimized formulations are described in the main text,  
136 and Supplementary Data. Paper tickets were prepared for liquid dispensing by directly attaching  
137 using adhesive (3M Super 77 Multipurpose Spray Adhesive) to a 384-well Thermofisher  
138 microwell plate (Thermofisher Catalog Number: 142761). Reaction components were dispensed  
139 directly onto the 384-well ticket using an Echo 525 acoustic liquid handler (Beckman Coulter) or  
140 multipipettor for volumes below 1000 nL and above 1000 nL, respectively. Unless otherwise  
141 noted all swH/trH tickets were prepared to contain a final concentration of 50 ng/μL pUCGA-trH-  
142 lacZ per reaction when resuspended in 2uL final volume. The Echo Plate Reformat software  
143 and custom scripts were used to prepare Echo transfer protocols. Reactions were lyophilized  
144 using a lyophilizer (VirTis AdVantage XL-70, SP Scientific) using a bell jar attachment. The shelf

145 was prechilled to  $-40\text{ }^{\circ}\text{C}$ , and the condenser to between  $-65$  and  $-70\text{ }^{\circ}\text{C}$ . The paper tickets  
146 were frozen for at least 5 min in a  $-80\text{ }^{\circ}\text{C}$  freezer. After removing the plate, it was immediately  
147 placed in the lyophilizer, the vacuum was activated, and the shelf temperature set to  $-20\text{ }^{\circ}\text{C}$   
148 overnight. The 384-well tickets were prepared for reading by attaching the ticket via adhesive  
149 directly to a 384-well plate that had been filled with  $30\text{ }\mu\text{L}$  of water per well. Ticket spots were  
150 resuspended in  $2\text{ }\mu\text{L}$  of  $50\text{ ng}/\mu\text{L}$  pUCGA-trH-lacZ DNA in diH<sub>2</sub>O using a multipipettor unless  
151 otherwise noted. Following rehydration, the plates were sealed with a plate cover from a  
152 microwell plate (Thermofisher Catalog Number: 142761), the edges wrapped in parafilm to  
153 prevent evaporation, and placed directly into a scanner for imaging (see Data Collection and  
154 Machine Vision Analysis section).

### 155 *DOE and Statistical Analysis*

156 All statistical analyses in this section were performed using Stat-Ease Design-Expert 13 and  
157 SAS JMP® Pro 15 software. To optimize the Cai reaction mixture, I-Optimal criterion was used  
158 to create optimal Mixture-Amount DOEs based on a quadratic statistical starting model. The  
159 design used a starting model that was quadratic on the mixture side and quadratic on the  
160 process side, with a “Kowalski-Cornell-Vining” (KCV) structure that restricted the crossing of the  
161 mixture and process term (amount) to 2-way. The design is capable of fitting non-linear  
162 blending effects up to second order. Within each of the 14 or 16 individual components for  
163 adding Cai or PANOx-SP components, respectively, the low and high limits varied by  
164 component. Additional details of the DOE models are available in the **Supplementary Results**  
165 and **Supplementary Data File**.

166  
167 For the heat tolerance optimization mixtures, I-Optimal criterion was used to create an optimal  
168 Mixture DOE based on the quadratic statistical starting model. The Mixture type DOE design

169 was selected in order to maximize experimental efficiency<sup>30</sup>. A quadratic starting model having  
170 the ability to characterize all linear blending effects for each of the individual 14 formulation  
171 components as well as all possible non-linear blending effects involving any pair of the 14  
172 formulation components was selected. For heat tolerance reactions, a formulation the 14  
173 individual components were limited to a range of 0 to 1000 nL. Additionally, each sample  
174 formulation was subject to a total volume of 3000 nL.

175

176 Functional Data Analysis (FDA) for both case studies was applied via the “Functional Data  
177 Explorer” platform within SAS JMP® Pro 15 software. A Functional Principle Components (FPC)  
178 decomposition was applied to the response curves, decomposing each curve into a Functional  
179 Principle Component “1” (FPC1) and Functional Principle Component “2” (FPC2) score where  
180 the FPC1 and FPC2 scores for an individual sample response curve represent the deviation  
181 from the overall mean response curve. A statistical model for the DOE generated was then fit to  
182 the FPC1 and FPC2 responses. Forward and backward step regression using the Akaike  
183 Information Criterion (AIC) was used to reduce the model for the FPC1 and FPC2 response,  
184 respectively. The R-Square Predicted metric was used along with the “check-points blends” (in-  
185 line validation samples) to validate the DOE based prediction models’ predictive capability.  
186 Optimization was performed using the Stat-Ease Design-Expert 13 Numerical Optimization  
187 feature in parallel with the SAS JMP® Pro 15 software Prediction Profiler Platform. Both  
188 softwares start with the DOE based prediction model and, after converting the FPC response to  
189 a zero to one desirability scale, use numerical methods to find the formulations that best  
190 optimize the response.



## 191 *Data Collection and Machine Vision Analysis*

192 Image processing from 384-well tickets was performed using three major steps. The ticket is  
193 placed on a flatbed scanner (Epson, Perfection V600 Photo) housed within an incubator to  
194 produce a time course of sensor images at 37 °C. Each plate is arranged on the scanner at an  
195 arbitrary point and scanned directly following rehydration. Custom software was used to capture  
196 raw 16-bit color images of the scanner bed at specified intervals. The series of images were  
197 then analyzed to monitor the biosensor's response over time using scripts that process the  
198 images as follows: time course images are placed in consistent orientation; spots are delineated  
199 from the image background and segmented into individual positions (**Figure S1**); average RGB  
200 value for each spot tile is computed; and the color change ( $\Delta E$ ) and hue values ( $\Delta H$ ) returned  
201 for each well within the context of CIELAB perceptual color space. For the purposes of this  
202 work, an arbitrary point of visibility was designated at  $\Delta E=10$  wherein experimenters agreed the  
203 color shift was very clear (**Figure S2**).

## 204 *3D-Printed Sensor Design.*

205 All designed parts were created in SolidWorks (SolidWorks) computer aided design software  
206 and exported as .stl files for slicing within the Ultimaker Cura software (Ultimaker). "Engineering  
207 – Normal" parameters were selected on Cura utilizing support for overhangs greater than 45°  
208 and without additionally printed build plate adhesion. Parts were printed using Ultimaker ABS  
209 and Ultimaker Breakaway Support filament on the Ultimaker S5 dual extrusion 3D printer. Prior  
210 to printing, the glass bed was pre-treated with AirWolf ABS adhesion solution prior to preheating  
211 the build plate to 125 °C. All paper layers were printed and prepared as described above prior to  
212 the addition of the cell-free extract mix. The agarose-topped layer was prepared by directly  
213 adding 5  $\mu$ L of 1.25% molten agarose to each paper spot. Each extract layer was prepared as  
214 described above. Both the cell-free extract layer and the agarose-topped layer were then frozen

215 at -80 °C and lyophilized as described above. Sensors were assembled by placing each layer  
216 on the sampling plate, adding a form fitted “quad” top plate over the agarose-topped layer, and  
217 covering the top with MicroAmp Clear Adhesive Film (Thermo Fisher). Sensors were tested  
218 through the addition of 25 µL of 50 ng/µL pUCGA-trH into the sample chamber and incubating in  
219 the flatbed scanner at 37 °C.

## 220 **Results and Discussion**

### 221 *High-Throughput Testing Platform of Paper-embedded Reactions*

222 Due to the labor-intensive nature of paper-based cell-free biosensor development, we reasoned  
223 that the development of a high-throughput testing platform to explore large combinatorial search  
224 spaces would accelerate improvement of their overall function. Paper-based reactions in the  
225 literature are typically prepared using biopsy punches to cut out small discs that are placed into  
226 microtiter plates or wax-printed paper tickets with modest numbers of wells; reactions are then  
227 spotted, lyophilized, and rehydrated, typically by hand (**Figure 1A**)<sup>26,27</sup>. While this method  
228 effectively creates portable sensors, it is not amenable to high-throughput experiments as even  
229 simple titrations of fixed reagents create a high-experimental load. For example, a more  
230 complex experiment using the excipients in this study to improve durability of a sensor to heat  
231 creates a combinatorial search space of 6,103,515,625 potential combinations when using only  
232 5 fixed concentrations (**Figure 1B**). To improve cell-free paper sensors testing throughput, we  
233 replicated the commonly used 384-well format using wax-printing on paper, yielding a  
234 127.76x85.47 mm 384-well paper ticket template with 3.5 mm diameter wells. Biologically  
235 inactive adhesive was used to apply the paper ticket over a standard 384-well plate, and an  
236 Echo 525 Acoustic Liquid Handler was used to transfer reaction components from an Echo  
237 source-plate to the sensor wells using standard Echo protocols. The tickets were then  
238 lyophilized, rehydrated using DNA, and CFE reaction activity measured by color change using a

239 flatbed scanner and custom machine vision and image analysis software, described in detail in  
 240 the methods, that extracts a measure of human-perceived color change ( $\Delta E$ ) (Figure 1C,  
 241 Figure S1).  
 242

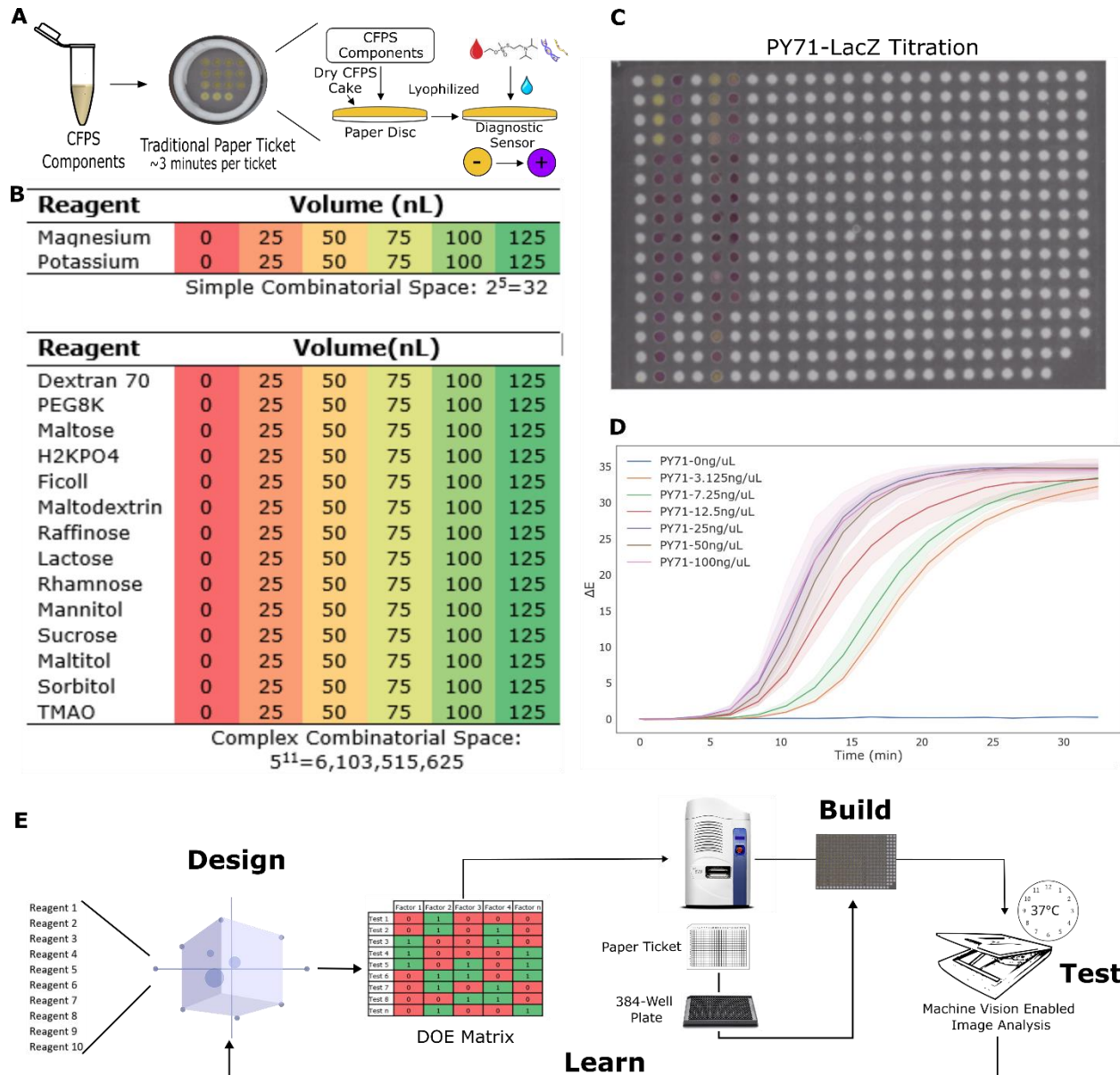


**Figure 1:** Optimizing paper-based cell-free reactions in high throughput. **A.** Cell-free components are lyophilized directly to a paper disc or ticket and rehydrated with an aqueous analyte to start protein production, in this case LacZ ( $\beta$ -galactosidase), to affect a color change from yellow to purple by cleavage of the CPRG substrate. **B.** An example experiment changing fixed concentrations of salts affecting CFE

*(top) and a more complex experiment assessing protective additives with 5 fixed concentrations (bottom). C. Representative image of 384-well wax-printed paper ticket. D. Traces of  $\Delta E$  from titrations of a plasmid encoding for constitutively expressed LacZ (pY71-LacZ) in the PANOx-SP CFE system extracted from time course images of a ticket. E. Graphic illustration of the DBTL cycle used to explore the combinatorial space of cell-free paper-ticket compositions. Initial tests of excipients and reagents defined an initial DOE matrix that was tested and the resulting data used to define a predictive model for active and optimal reagent concentrations.*

243

244 **Figure 1C** shows a representative 384-well ticket with reactions expressing LacZ ( $\beta$ -  
245 galactosidase), an eye-readable colorimetric reporter that has been used in a wide range of  
246 applications<sup>28</sup>. As an initial validation of the approach, we performed a titration curve of a  
247 plasmid (pY71-LacZ) that constitutively expresses LacZ from the strong T7 promoter. For these  
248 initial tests, the PANOx-SP formulation was used. The reactions were dispersed onto a 384-well  
249 ticket as a master mix with only the plasmid dispersed separately; the ticket was then lyophilized  
250 and rehydrated using water. The titration resulted in increasing rates of LacZ production  
251 commensurate with the concentration of the DNA transferred, plateauing at 25 ng/ $\mu$ L, which is  
252 consistent with prior work indicating a saturation of translational machinery in the CFE reaction  
253 **(Figure 1D)**<sup>29</sup>.

254

255 To explore the vast combinatorial space inherent to non-fixed quanta we decided to employ  
256 exploratory DOE with an objective function geared towards improving the rate of our cell-free  
257 reactions **(Figure 1D)**. The first day of our DBTL cycle is initiated with an exploratory DOE using  
258 a list of excipients and additives using volumes ranging from 25 to 1000 nL. The reaction  
259 compositions in the exploratory DOE are transferred to the Echo, dispensed on to a 384-well  
260 paper ticket, and lyophilized overnight. On the second day, the samples are rehydrated, placed  
261 onto a flatbed scanner, color change data extracted, and the resulting data fit to the DOE model.

262 The loop is then restarted with optimized reaction conditions predicted by the model to be run  
263 with replicates. DOE offers the ability to efficiently and simultaneously characterize the influence  
264 that each formulation component has on the response of interest while at the same time testing  
265 for interactions between formulation components and process factors. This is a distinct  
266 advantage of DOE experimentation over “one factor at a time” experimentation as we are able  
267 to reduce the multidimensionality of the problem to a manageable number of potential test  
268 cases. The method allows for large amounts of data to be gathered, analyzed, and fitted to an  
269 empirical statistical model that can serve as a prediction for a response at any possible  
270 combination of formulation components within the entire design.

271

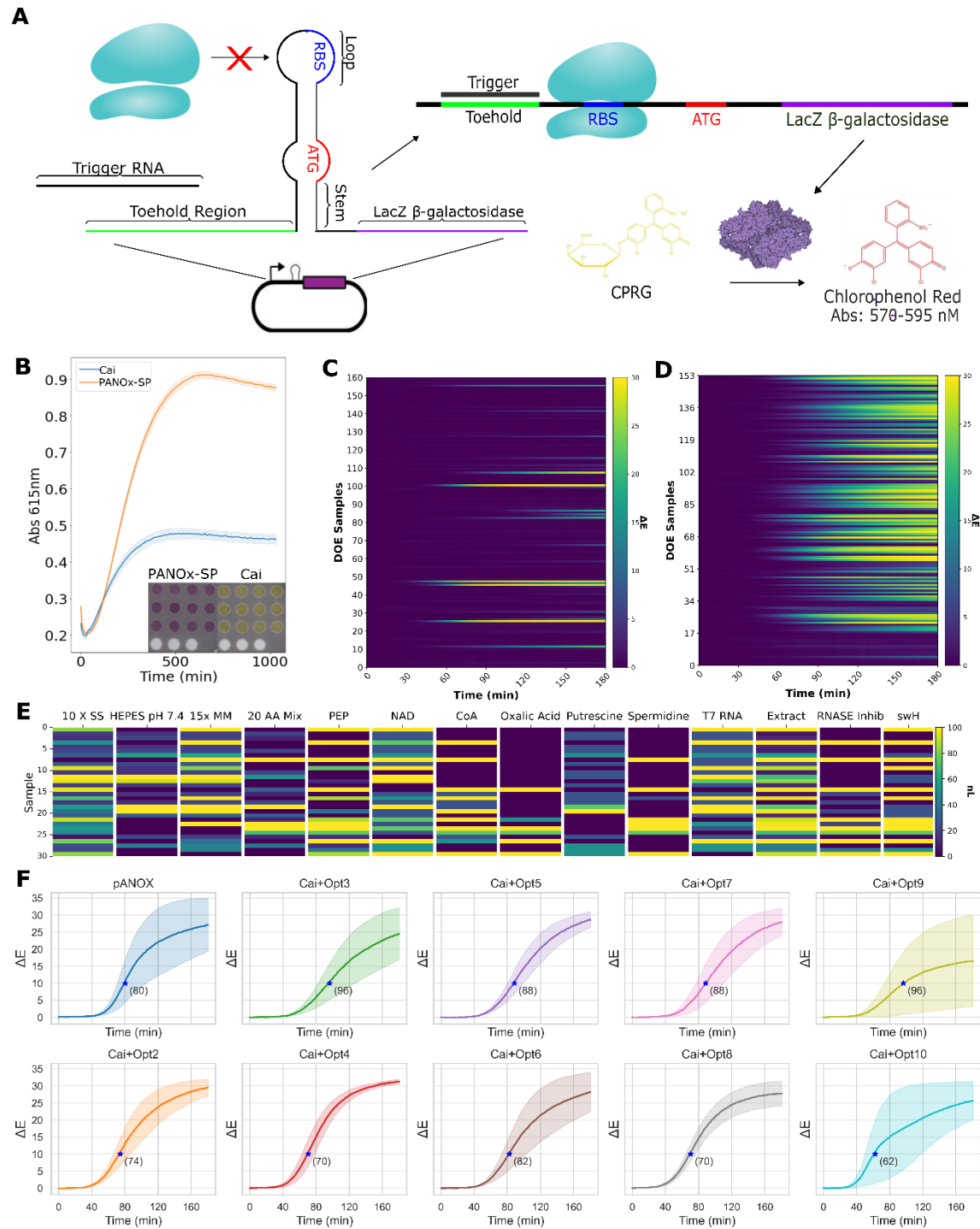
### 272 *Optimization of a Low-Cost CFE Mix*

273 As a model diagnostic sensor for the remainder of this work, we used a lyophilized CFE reaction  
274 containing a toehold switch plasmid (pUCGA-swH-lacZ) that expresses LacZ in the presence of  
275 a target trigger RNA. The biosensor reactions are rehydrated by the addition of a plasmid that  
276 constitutively expresses the cognate trigger RNA (pUCGA-trH) (**Figure 2A**). Lyophilized tickets  
277 with identical spots containing 50 ng/μL of pUCGA-swH-lacZ were activated using varying levels  
278 of pUCGA-trH (**Figure S3**). We further tested our ability to dispense reagents by measuring the  
279 transfer and subsequent effect of more viscous reagents. RNASE inhibitor has been noted as  
280 being important to the function of cell-free paper-based biosensors due to the natural presence  
281 of nucleases on the matrix<sup>10,30</sup>. We titrated the concentration of RNASE inhibitor both to  
282 measure the ideal concentration of a critical component and to assess the platform's ability to  
283 modulate a viscous reagent. RNASE inhibitor Murine dissolved in 50% glycerol was titrated onto  
284 identical CFE reactions, lyophilized, and resuspended in 50 ng/μL of both pUCGA-swH-lacZ and  
285 pUCGA-trH. Increasing concentrations of RNASE inhibitor improved the rate of the reaction,

286 with doubling the typical concentration of RNASE inhibitor to 2.4 units/ $\mu$ L providing the best  
287 reaction rate and a loss of benefit at 4.8 units/ $\mu$ L (**Figure S4**).

288

289 A minimized version of the Cytomim CFE system as reported on by Cai and colleagues  
290 demonstrated the ability to drop the materials cost of a CFE system by an order of magnitude  
291 through the removal of non-essential and expensive components<sup>17</sup>. At a total cost of ~\$445/L,  
292 the reaction mixture published by Cai heretofore referred to as the Cai reaction mixture is  
293 significantly cheaper than the ~\$5,570/L cost of the traditionally used PANOx-SP mixture (**Table**  
294 **S1**)<sup>29</sup>. This is relevant both for the purposes of making the biosensors affordable in the context  
295 of low-resource point-of-need applications and to limit the need for components such as tRNAs,  
296 nucleotide triphosphates, and volatile energy sources such as PEP that can be difficult to  
297 acquire when supply chains are disrupted. However, we found Cai CFE reactions to produce no  
298 clear color change when used with our paper-based biosensors, despite functioning in liquid  
299 reactions (**Figure 2B**). We sought to resolve this limitation as well as reduce the cost per test by  
300 optimizing a cheap but inactive-on-paper cell-free energy mixture to function with paper  
301 sensors.



302

**Figure 2: Optimization of low-cost CFE reactions for performance in paper-based biosensor reactions. A.** The presence of trigger RNA disrupts the stem-loop structure of the switch RNA and allows for translation of LacZ ( $\beta$ -galactosidase). **B.** Comparison of PANOx-SP and Cai CFE biosensor reactions in a liquid format in plates; (**inset**) the same reaction components in the paper-based biosensor format after a 3 h

*incubation C. DOE heatmap produced from the addition of Cai reaction components to the baseline Cai CFE formulation. D. Similar experiment was performed using PANOX-SP reaction components added to the baseline Cai formulation. E. Heatmap of compositions of the 30 optimal mixtures predicted from DOE analysis. F. Time courses of paper tickets using predicted optimized mixtures adding PANOX-SP reagents to baseline Cai mixture. Blue stars indicate the point at which the paper ticket reaction reached  $\Delta E \geq 10$ . Standard deviations shown as shadows on each trace were derived from triplicate reactions.*

303

304 We hypothesized that the absence or low concentration of one or more critical components  
305 resultant from the cost-minimization efforts was a likely cause of the inability of the Cai to  
306 function on paper. To test this hypothesis, we designed a DOE framework to add combinations  
307 of components of the Cai formulation by dispensing them directly on 384-well tickets containing  
308 normal Cai reactions (Methods). The tickets were then lyophilized to both to normalize the final  
309 reaction volumes and because lyophilization is an important aspect of real-world applications of  
310 the technology. After rehydration, color change traces were extracted as previously. Though our  
311 machine vision approach is capable of quantifying small shifts in color, a threshold of  $\Delta E \geq 10$   
312 was used to note a point at which the reactions became obviously visible by eye and served as  
313 a barometer for sensor function for the remainder of this study (**Figure S2**). We prepared an  
314 initial 16-component DOE using the components of the standard Cai mix, adding variable  
315 amounts of each component in volumes ranging from 0-1000 nL (**Figure 2C**; **Table S5**). While  
316 some combinations of added reagents did produce detectable signal, the data was not sufficient  
317 to fit the DOE model and make predictions of optimal formulations. Following these results, we  
318 speculated that some component(s) of the PANOX-SP mix might explain the poor relative  
319 performance of the Cai mix compared to PANOX-SP on paper tickets. We next used a 153-  
320 sample framework adding variable amounts of 14 PANOX-SP components to baseline Cai  
321 reactions (**Table S4**). Many of these combinations showed a marked improvement in the  
322 function of the Cai mix on paper sensors (**Figure 2D**). Additional details about the DOE, data



323 processing, and results are available in the **Supplementary Results, Figures S5-7,** and  
324 **Tables S7-8.**

325

326 Our initial DOE model generated 30 optimal reaction mixtures that spanned diverse  
327 combinations of added components (**Figure 2E**). We test the top 10 predicted optimals and  
328 each reached the threshold for visibility within 1.5 hrs, except for Cai-Opt1 which was inactive  
329 (data not shown) (**Figure 2F**). Nine formulations were active and with statistically no difference  
330 in speed when compared to the PANOx-SP controls (**Table S9**). These formulations further had  
331 costs ranging from \$0.0013-\$1.96 per 1  $\mu$ L reaction added to \$0.00044 for baseline Cai; these  
332 costs range from ~43-fold cheaper to 35-fold more expensive than the \$0.056 for PANOx-SP,  
333 with higher costs driven almost entirely by additional DNA (**Table S10**). Here we predicted  
334 optimal formulations purely based on performance; it is likely that these costs could be driven  
335 down further by instead predicting formulations that maximize performance per unit cost.

336

337 Analyzing the combinations of additives that result in high performing formulations do not  
338 provide simple, obvious intuition into the determinants of improved performance. Notably, all 14  
339 components appeared at both the highest and lowest levels in at least one of the 30 predicted  
340 optimal formulations, though some do appear more frequently. By considering the blending  
341 coefficients for the first and second order effects predicted by the model to have the greatest  
342 impact, it is clear that none of the components in isolation explain the improvements in  
343 performance (**Table S7**). The second order effects offer scant additional insight and instead  
344 highlight the complexity of the system (**Table S8**). For example, spermidine appears in 4 of the  
345 10 strongest estimated second order effects both as a negative effector (with T7 RNAP and  
346 HEPES) and as a positive effector (with RNASE inhibitor and 20 AA Mix). It is worth pointing out  
347 that the DOE approach makes no attempt to model the complete system; instead, it aggregates  
348 estimates of first and second order effects in a way that can find improved performance after

349 testing only a tiny fraction of a large search space. Moreover, interpretation of the effects of  
350 individual components is complicated by the Mixture-Amount design wherein constraints on the  
351 total amounts added mean that changing one variable necessitates changing others  
352 simultaneously. One noteworthy observation is that the model estimates that RNASE inhibitor  
353 provides a positive effect in combination with Spermidine, CoA, and PEP, but a small negative  
354 effect alone, suggesting that our earlier conclusion that additional RNASE inhibitor improves the  
355 reaction for the PANOx-SP system is dependent on one or more specific components in the  
356 mix. Ultimately, despite providing limited insights into the inner workings of the system, the  
357 model reliably predicted diverse, high-performing formulations. Until mechanistic models are  
358 developed that can fully capture the highly complex dynamics of CFE reactions, DOE offers a  
359 powerful tool to rapidly optimize formulations for a particular use case.

360

### 361 *Engineering Cell-Free Biosensor Heat Tolerance*

362 The need for biosensors in austere environments inherently requires that the biological systems  
363 are capable of functioning outside ideal laboratory conditions. For instance, high salt,  
364 temperature, or pH environments can deactivate biological sensors. These problems can be  
365 magnified if the tools in question require notoriously difficult to maintain cold chains. We sought  
366 to improve the robustness of our sensors to elevated temperatures during storage through the  
367 addition of excipients with previously reported impacts on the function of lyophilized products  
368 following exposures to environmental stresses (**Table S6**).

369

370 During the sublimation process, the disruption of hydrogen bonding pairs can result in protein  
371 aggregation. To resolve this issue, excipients are often added to purified protein components in  
372 order to stabilize electrostatic complexes during drying. Additionally, exposure to temperatures

373 above a protein's melting temperature can unfold regions with thermodynamically unfavorable  
374 refolding and lead to aggregation and ultimately inactivity of the biosensor. Preliminary  
375 experiments with paper biosensors using the PANOx-SP system exposed to 6 hr incubation at  
376 50 °C were found to be completely inactive (data not shown). We hypothesized that an effective  
377 combination of excipients to improve heat tolerance could be found by applying a DOE analysis  
378 to the lyophilization and heat testing process. We produced a DOE matrix testing combinations  
379 of 14 excipients shown to provide protective effects in other studies<sup>15,32-35</sup> by adding them to the  
380 baseline PANOx-SP system and measuring the activity following heat challenges. An initial 6 hr  
381 incubation at 50 °C showed several reactions with a substantial improvement in the heat  
382 tolerance (**Figure 3A**).



385

386 Unlike the prior optimization, there were clear trends in the components that appeared in  
387 predicted optimal formulations: some excipients (e.g. PEG, lactose, and rhamnose) appeared  
388 rarely or not at all in the predicted top formulations, while others (e.g. H<sub>2</sub>KPO<sub>4</sub>, Ficoll, and  
389 Raffinose) appeared frequently (**Figure 3B**). Considering the linear and non-linear blending  
390 coefficients for the model, however, again yields a complicated picture (**Tables S11-12**). For  
391 example, while PEG, lactose, and rhamnose had relatively strong negative linear effects,  
392 PEG+rhamnose and lactose+rhamnose had relatively strong positive effects. This observation  
393 is explained by how the coefficients are weighted to predict the FPC1 value according to our  
394 Mixture-Amount constraints. More specifically, component amounts are pseudo-coded to range  
395 from 0 to 0.333 such that no single component can go above 1000 nL out of a maximum  
396 allowed 3000 nL total amount. For the example of PEG, lactose, and rhamnose added at  
397 maximum amounts, the predicted FPC1 value is calculated as:

398

$$\begin{aligned} \text{FPC1}_{\text{Predicted}} &= \frac{1}{3} \sum_{\substack{\text{PEG,} \\ \text{lactose,} \\ \text{rhamnose}}} \text{Linear blending coefficients} + \frac{1}{9} \sum_{\substack{\text{PEG,} \\ \text{lactose,} \\ \text{rhamnose}}} \text{Non-linear blending coefficients} \\ &= \frac{1}{3}(-248.4 - 290.8 - 126.1) + \frac{1}{9}(0 + 1453.4 + 1158.8) = 68.5 \end{aligned}$$

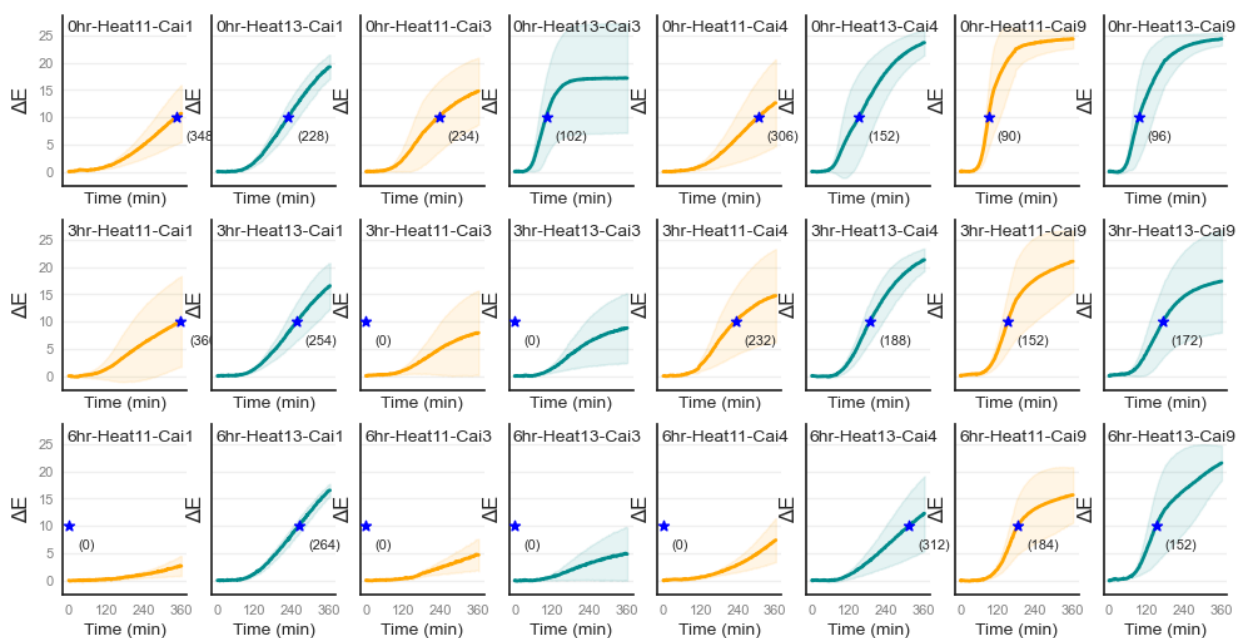
401

402 Since 68.5 is much low compared to the predicted optimals (e.g. #30 is predicted at 205.3), this  
403 apparent discrepancy is clarified. This observation can be interpreted as PEG, lactose, and  
404 rhamnose each having negative effects alone, with rhamnose having synergistic effects with  
405 both PEG and lactose that do not overcome the negative individual effects. While deeper  
406 insights into how these complex formulations perform would be highly welcome, as discussed  
407 above, the purpose of the DOE approach is to predict optimal formulations despite limited  
408 understanding of the system.

409  
410 Fourteen predicted optimal formulations along with the top performing formulation from the  
411 exploratory DOE were further tested in quadruplicate by exposing the tickets to a 6 h incubation  
412 at 50 °C (**Figure 3C**). Notably, several of these reactions appeared to perform favorably to  
413 untreated PANOx-SP samples from the Cai optimization experiments (**Figure 2F**), though we  
414 did not include that control to enable a direct comparison. We nonetheless checked the  
415 statistical significance of these apparent improvements (run on different tickets on different  
416 days) and found no significant difference in time to reach a  $\Delta E \geq 10$  for any of the optimal  
417 formulations compared to PANOx-SP, which is unsurprising given substantial variability  
418 between replicates (**Table S11**; see discussion on variability below). While the Heat-Opt11  
419 formulation reached the  $\Delta E$  threshold for visibility at 47 min, the best reported in this study, it is  
420 not clear if the additives truly improved the performance of the base PANOx-SP. While we did  
421 not further explore the performance impact of these additives without heat exposure, other work  
422 has noted the dual purpose of maltodextrin as a lyoprotectant and energy source, suggesting  
423 that such improvements are possible.

424  
425 Following our success optimizing the low-cost extract and improving the heat tolerance of our  
426 paper ticket sensors, we sought to merge the two-systems by evaluating the effect of adding the  
427 heat tolerance excipients optimized for the expensive PANOx-SP reaction mixture to our  
428 optimized Cai formulations. We chose 4 optimized Cai formulations (Cai-Opt3 and 9 that use  
429 minimal added DNA and Cai-Opt1 and 4 that add maximum DNA) and 2 optimized heat-  
430 tolerance formulations (Heat-Opt 11 and 13 for the fastest mean time to  $\Delta E \geq 10$ ) and exposed  
431 pairwise combinations of these formulations on tickets to 50 °C for 0, 3, or 6 h (**Figure 4** and  
432 **Tables S9, S13**). We found that even without heat exposure, all combinations except the two  
433 involving Cai-Opt9 performed poorly but were still active; after heat exposure those  
434 combinations performed progressively worse, with four of the six combinations never reaching

435  $\Delta E \geq 10$  after 6 h exposure to 50 °C. Both combinations involving Cai-Opt9, however, performed  
 436 similarly to the earlier PANOx-SP controls (mean time to  $\Delta E \geq 10$  of 80, 90, and 96 min for  
 437 PANOx-SP, Heat11+Cai9, and Heat13+Cai9, respectively), and retaining some activity after  
 438 heat exposure (mean time to  $\Delta E \geq 10$  ranging from 152 to 184 min). Further work would likely  
 439 uncover combinations that provide better heat tolerance while maintaining low costs.



440

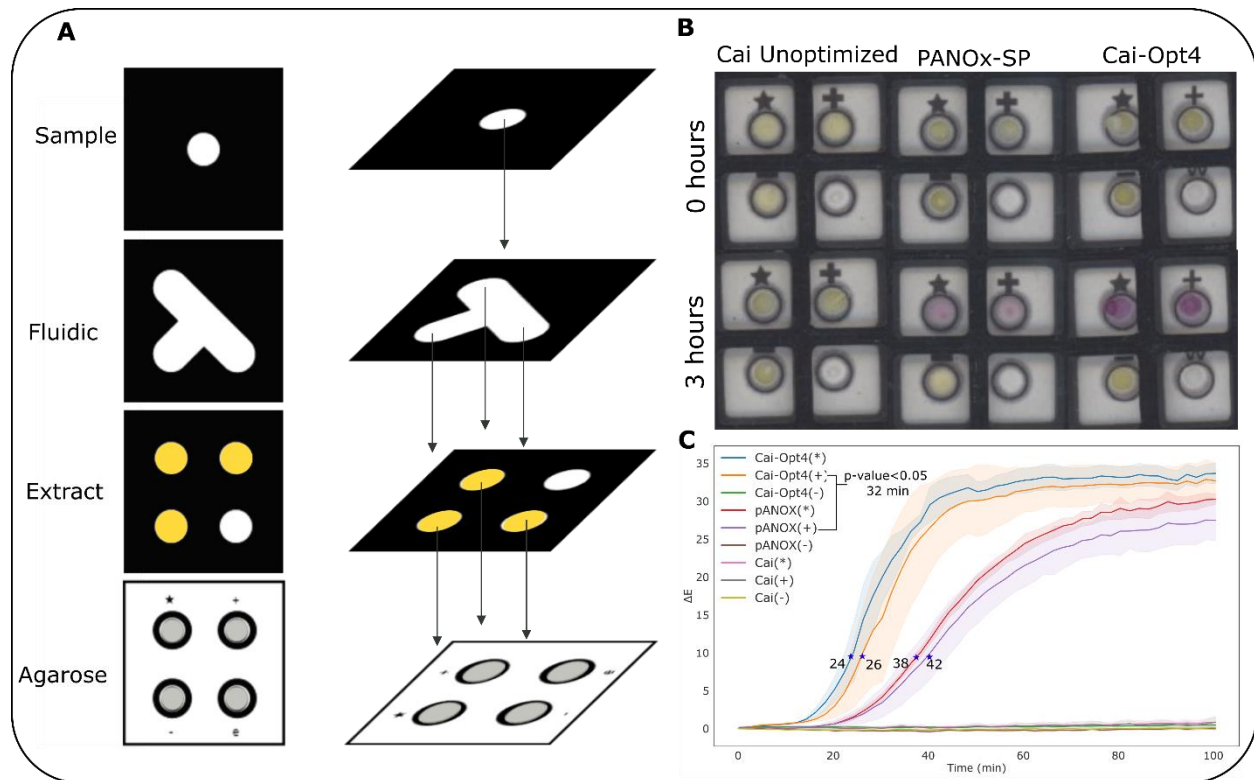
**Figure 4.** Heat tolerance of combinations of optimized Cai formulations and heat-tolerance excipient combinations optimized using PANOx-SP as the baseline. Combinations of Cai-Opt1, 3, 4, and 9 and Heat-Opt11 and 13 were added to baseline Cai on tickets and exposed to 50°C for 0, 3, or 6 h. Shaded error bars are one standard deviation from  $n=4$  replicates. A blue star indicates the time at which the cell-free biosensor reached a  $\Delta E$  of 10; if no replicates reached the threshold, a value of 0 is shown.

441 Handheld Biosensors Effectively Make use of Optimized CFPS Mixtures

442 To showcase the effectiveness of our optimized reactions, we designed and created a handheld  
 443 paperfluidic device to show the potential of the colorimetric sensor as a diagnostic tool. A 4-

444 layer wax-printed paperfluidic sensor housed in a 3D-printed cassette (**Figure 5A, Figure S8**)  
445 was built using either the unoptimized Cai mix, PANOx-SP, or an optimized version of the Cai  
446 mix (Cai+Opt4) and tested by flowing pUCGA-trH plasmid through the device. As expected, the  
447 Cai mixture without optimization did not produce any detectable result, whereas both the  
448 PANOx-SP and the optimized Cai reaction mixtures were all visible within 42 minutes (**Figure**  
449 **5B-C**). Interestingly, the optimized Cai mixtures led to a faster time to visibility than the standard  
450 PANOx-SP system ( $\Delta E \geq 10$  at 26 vs 42 mins, respectively;  $p=0.034$ ), becoming statistically  
451 differentiable at 32 min ( $p < 0.05$ ). These reaction times outpace the 384-well ticket apparatus  
452 ( $\Delta E \geq 10$  at 80 vs 88 min for PANOx-SP and Cai-Opt4, respectively; **Figure 2F**), indicating that  
453 the handheld biosensor system improves the function of the CFE reaction both in general and  
454 differentially for the optimized formulation. Notable differences are sealing of the device to limit  
455 evaporation and the presence of an agarose-hydrogel layer intended to enhance flow in the  
456 paperfluidic system. Given that hydration of the reaction mixture can be crucial to function, both  
457 of these factors likely help to maintain an environment more amenable to the CFE reactions<sup>31</sup>.  
458 This observation shows the importance of the physical and environmental factors that can  
459 modify the function of cell-free biosensors and opens new avenues for further research and  
460 development. Rehydration, dilution of the components, and variable environmental humidity and  
461 temperature have all been shown to be critical factors, especially in the context of biological  
462 sensing<sup>36</sup>. This work further incentivizes context-specific modifications for biological sensing  
463 platforms as directly porting one reaction mixture to a different context can have unintended  
464 consequences.





465

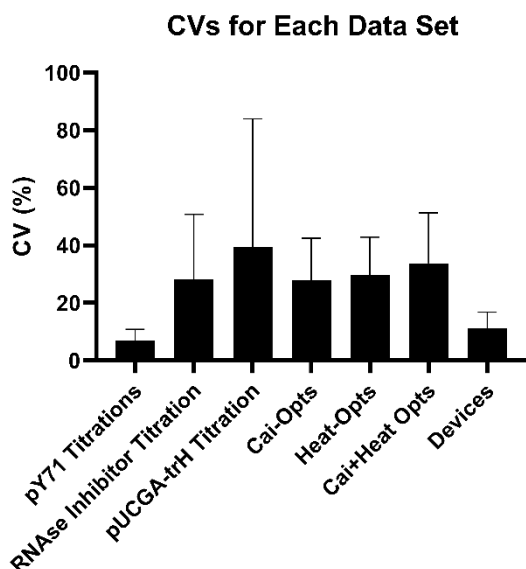
466 **Figure 5.** Performance of optimized biosensors in a fieldable paperfluidic device. **A.** Schematic of a wax-  
467 printed paperfluidic device wherein sample is added to the sample layer, disseminated using a paper  
468 fluidic layer to the individual reaction chambers containing cell-free extract, and visualized on an agarose-  
469 topped layer held together by a 3D printed holder (**Figure S8**). The “★” indicates a sample chamber with  
470 a CFE reaction and pUCGA-swH-lacZ; “+” indicates a positive control containing a CFE reaction with both  
471 pUCGA-swH-lacZ and pUCGA-trH plasmids; “-” indicates a negative control containing a CFE reaction  
472 with no DNA; and “e” being an empty node intended to identify any leaking between layers. Both the top  
473 and bottom layer 3D-printed enclosures are sealed with transparent film following sample addition. **B.**  
474 Assembled sensor devices were imaged and analyzed using the same scanning rig and software as  
475 above. **C.** Time courses of three replicate devices. The shadow indicates one standard deviation. Blue  
476 stars indicate time to cross  $\Delta E \geq 10$ . One tailed T-test shows statistically significant difference compared to  
477 negative controls at 32 min for Cai-Opt4 and PANOx-SP sample reactions.

478

## 479 *Assessment of Variability*

480 In the initial tests of our experimental platform titrating pY71-LacZ plasmid, we observed  
481 reasonably consistent error bars (**Figure 1D**). In later cases, however, we found that error bars  
482 for replicate experiments were larger, resulting in a lack of statistical significance between  
483 conditions even when differences in means appear large, e.g. the previously discussed  
484 differences between the heat-tolerance optimal formulations and PANOx-SP. We therefore  
485 assessed the CV of time to  $\Delta E \geq 10$  across all data sets (**Figure 6**). We found that the initial  
486 pY71-LacZ titrations were anomalously consistent (CV=6.9%) compared to other 384-well ticket  
487 experiments (CV=28.0-39.5%). Previous efforts to measure variability of CFE reactions has  
488 found that ~6-10% is typical for a single experimenter across days when prepared by hand,  
489 suggesting that the substantial increase in variability is a result of small volume dispensing  
490 errors either from the acoustic liquid handler or baseline master mixes. More careful calibration  
491 and validation of proper dispensing would be needed to validate this hypothesis and  
492 subsequently mitigate any issues. Other possibilities are that time to  $\Delta E \geq 10$  using an enzymatic  
493 reporter is more variable than the endpoint GFP fluorescence used in the other studies or that  
494 something about the paper ticket format increases variability; however, because in one case we  
495 saw similar consistency, we suspect dispensing errors are more likely to be the cause. While  
496 such variability limits fine tuning of reaction compositions, our results show that rapid, efficient  
497 screening through very large combinatorial design spaces is still viable. We note also that the  
498 average variability in our device format was 11.2%, indicating that optimal formulations can  
499 perform reasonably consistently in a more applied setting.

500



501  
502 **Figure 6:** Variability within replicates across experiments in this study. Bars represent the average within-  
503 replicate CV across each experiment list. Error bars represent one standard deviation.

504

## 505 **Conclusions**

506 Scaling the production of cell-free biological sensors requires cost-effective and stable methods  
507 of producing them as diagnostic tools. This work shows how high throughput experimentation  
508 driven by DOE can rapidly identify substantial improvements in performance at low costs and  
509 with tolerance to heat exposure in paper formats relevant to application. Given the complexity of  
510 these formulations, traditional optimizations varying one or two variables at a time are  
511 intractable; with the approaches outlined here, a single researcher can reduce enormous search  
512 spaces to a manageable number of experiments that can be executed in two consecutive days.  
513 The ability to then immediately port these improvements into a fieldable diagnostic device from  
514 low-cost, easy-to-produce components underscores the potential for such sensors to have real  
515 world impact. We anticipate that continued development of new CFE sensors paired with further

516 improvements to the performance, cost, stability, and deployability of CFE reactions will lead to  
517 the technology achieving its potential impact.

518

## 519 **Acknowledgments**

520 Funding was provided by a congressional program titled Cell-free Biomanufacturing. This  
521 project was supported in part by an appointment to the NRC Research Associateship Program  
522 at DEVCOM Chemical Biological Center for DCG administered by the Fellowships Office of the  
523 National Academies of Sciences, Engineering, and Medicine.

## 524 **Author Contributions**

525 DCG: Conceptualization, Methodology, Investigation, Data curation, Writing – Original Draft;  
526 JPD: Methodology, Formal analysis; CED: Software; DAP: Methodology; AEM: Methodology,  
527 Supervision; MWL: Conceptualization, Writing - Review & Editing, Supervision, Project  
528 administration, Funding acquisition.

## 529 **References**

- (1) Lavickova, B.; Maerkl, S. J. A Simple, Robust, and Low-Cost Method To Produce the PURE Cell-Free System. *ACS Synth. Biol.* 2019, 8 (2), 455–462. <https://doi.org/10.1021/acssynbio.8b00427>.
- (2) Dopp, B. J. L.; Tamiev, D. D.; Reuel, N. F. Cell-Free Supplement Mixtures: Elucidating the History and Biochemical Utility of Additives Used to Support in Vitro Protein Synthesis in E. Coli Extract. *Biotechnology Advances* 2019, 37 (1), 246–258. <https://doi.org/10.1016/j.biotechadv.2018.12.006>.
- (3) Amalfitano, E.; Karlikow, M.; Norouzi, M.; Jaenes, K.; Cicek, S.; Masum, F.; Sadat Mousavi, P.; Guo, Y.; Tang, L.; Sydor, A.; Ma, D.; Pearson, J. D.; Trcka, D.; Pinette, M.; Ambagala, A.; Babiuk, S.; Pickering, B.; Wrana, J.; Bremner, R.; Mazzulli, T.; Sinton, D.; Brumell, J. H.; Green, A. A.; Pardee, K. A Glucose Meter Interface for Point-of-Care Gene Circuit-Based Diagnostics. *Nat Commun* 2021, 12 (1), 724. <https://doi.org/10.1038/s41467-020-20639-6>.
- (4) Pardee, K.; Green, A. A.; Ferrante, T.; Cameron, D. E.; Daleykeyser, A.; Yin, P.; Collins, J. J. Paper-Based Synthetic Gene Networks. *Cell* 2014, 159 (4), 940–954. <https://doi.org/10.1016/j.cell.2014.10.004>.

- (5) Beabout, K.; Bernhards, C. B.; Thakur, M.; Turner, K. B.; Cole, S. D.; Walper, S. A.; Chávez, J. L.; Lux, M. W. Optimization of Heavy Metal Sensors Based on Transcription Factors and Cell-Free Expression Systems. *ACS Synth. Biol.* 2021, 10 (11), 3040–3054. <https://doi.org/10.1021/acssynbio.1c00331>.
- (6) McNerney, M. P.; Zhang, Y.; Steppe, P.; Silverman, A. D.; Jewett, M. C.; Styczynski, M. P. Point-of-Care Biomarker Quantification Enabled by Sample-Specific Calibration. *Sci. Adv.* 2019, 5 (9), eaax4473. <https://doi.org/10.1126/sciadv.aax4473>.
- (7) Sadat Mousavi, P.; Smith, S. J.; Chen, J. B.; Karlikow, M.; Tinafar, A.; Robinson, C.; Liu, W.; Ma, D.; Green, A. A.; Kelley, S. O.; Pardee, K. A Multiplexed, Electrochemical Interface for Gene-Circuit-Based Sensors. *Nat. Chem.* 2020, 12 (1), 48–55. <https://doi.org/10.1038/s41557-019-0366-y>.
- (8) Pandi, A.; Grigoras, I.; Borkowski, O.; Faulon, J.-L. Optimizing Cell-Free Biosensors to Monitor Enzymatic Production. *ACS Synth. Biol.* 2019, 8 (8), 1952–1957. <https://doi.org/10.1021/acssynbio.9b00160>.
- (9) Whitfield, C. J.; Banks, A. M.; Dura, G.; Love, J.; Fieldsend, J. E.; Goodchild, S. A.; Fulton, D. A.; Howard, T. P. Cell-Free Protein Synthesis in Hydrogel Materials. *Chem. Commun.* 2020, 56 (52), 7108–7111. <https://doi.org/10.1039/D0CC02582H>.
- (10) Hunt, J. P.; Zhao, E. L.; Free, T. J.; Soltani, M.; Warr, C. A.; Benedict, A. B.; Takahashi, M. K.; Griffiths, J. S.; Pitt, W. G.; Bundy, B. C. Towards Detection of SARS-CoV-2 RNA in Human Saliva: A Paper-Based Cell-Free Toehold Switch Biosensor with a Visual Bioluminescent Output. *New Biotechnology* 2022, 66, 53–60. <https://doi.org/10.1016/j.nbt.2021.09.002>.
- (11) Pardee, K. Perspective: Solidifying the Impact of Cell-Free Synthetic Biology through Lyophilization. *Biochemical Engineering Journal* 2018, 138, 91–97. <https://doi.org/10.1016/j.bej.2018.07.008>.
- (12) Sharpes, C. E.; McManus, J. B.; Blum, S. M.; Mgboji, G. E.; Lux, M. W. Assessment of Colorimetric Reporter Enzymes in the PURE System. *ACS Synth. Biol.* 2021, 10 (11), 3205–3208. <https://doi.org/10.1021/acssynbio.1c00360>.
- (13) Arce, A.; Guzman Chavez, F.; Gandini, C.; Puig, J.; Matute, T.; Haseloff, J.; Dalchau, N.; Molloy, J.; Pardee, K.; Federici, F. Decentralizing Cell-Free RNA Sensing With the Use of Low-Cost Cell Extracts. *Front. Bioeng. Biotechnol.* 2021, 9, 727584. <https://doi.org/10.3389/fbioe.2021.727584>.
- (14) Karig, D. K.; Bessling, S.; Thielen, P.; Zhang, S.; Wolfe, J. Preservation of Protein Expression Systems at Elevated Temperatures for Portable Therapeutic Production. *J. R. Soc. Interface.* 2017, 14 (129), 20161039. <https://doi.org/10.1098/rsif.2016.1039>.
- (15) Gregorio, N. E.; Kao, W. Y.; Williams, L. C.; Hight, C. M.; Patel, P.; Watts, K. R.; Oza, J. P. Unlocking Applications of Cell-Free Biotechnology through Enhanced Shelf Life and Productivity of *E. Coli* Extracts. *ACS Synth. Biol.* 2020, 9 (4), 766–778. <https://doi.org/10.1021/acssynbio.9b00433>.
- (16) Smith, M. T.; Berkheimer, S. D.; Werner, C. J.; Bundy, B. C. Lyophilized *Escherichia Coli* -Based Cell-Free Systems for Robust, High-Density, Long-Term Storage. *BioTechniques* 2014, 56 (4), 186–193. <https://doi.org/10.2144/000114158>.
- (17) Cai, Q.; Hanson, J. A.; Steiner, A. R.; Tran, C.; Masikat, M. R.; Chen, R.; Zawada, J. F.; Sato, A. K.; Hallam, T. J.; Yin, G. A Simplified and Robust Protocol for Immunoglobulin Expression in *E. Scherichia Coli* Cell-free Protein Synthesis Systems. *Biotechnology Progress* 2015, 31 (3), 823–831. <https://doi.org/10.1002/btpr.2082>.
- (18) Jeong, S.; González-Grandío, E.; Navarro, N.; Pinals, R. L.; Ledesma, F.; Yang, D.; Landry, M. P. Extraction of Viral Nucleic Acids with Carbon Nanotubes Increases SARS-CoV-2 Quantitative Reverse Transcription Polymerase Chain Reaction Detection Sensitivity. *ACS Nano* 2021, 15 (6), 10309–10317. <https://doi.org/10.1021/acsnano.1c02494>.

- (19) Brouillette, M. Repurposing the Cell Engine: Northwestern Announces the Cell-Free Biomanufacturing Institute. *GEN Biotechnology* 2022, 1 (3), 218–221. <https://doi.org/10.1089/genbio.2022.29037.mbr>.
- (20) Borkowski, O.; Koch, M.; Zettor, A.; Pandi, A.; Batista, A. C.; Soudier, P.; Faulon, J.-L. Large Scale Active-Learning-Guided Exploration for in Vitro Protein Production Optimization. *Nat Commun* 2020, 11 (1), 1872. <https://doi.org/10.1038/s41467-020-15798-5>.
- (21) Moore, S. J.; MacDonald, J. T.; Wienecke, S.; Ishwarbhai, A.; Tsipa, A.; Aw, R.; Kylilis, N.; Bell, D. J.; McClymont, D. W.; Jensen, K.; Polizzi, K. M.; Biedendieck, R.; Freemont, P. S. Rapid Acquisition and Model-Based Analysis of Cell-Free Transcription–Translation Reactions from Nonmodel Bacteria. *Proc. Natl. Acad. Sci. U.S.A.* 2018, 115 (19). <https://doi.org/10.1073/pnas.1715806115>.
- (22) Karim, A. S.; Dudley, Q. M.; Juminaga, A.; Yuan, Y.; Crowe, S. A.; Heggstad, J. T.; Garg, S.; Abdalla, T.; Grubbe, W. S.; Rasor, B. J.; Coar, D. N.; Torculas, M.; Krein, M.; Liew, F.; Quattlebaum, A.; Jensen, R. O.; Stuart, J. A.; Simpson, S. D.; Köpke, M.; Jewett, M. C. In Vitro Prototyping and Rapid Optimization of Biosynthetic Enzymes for Cell Design. *Nat Chem Biol* 2020, 16 (8), 912–919. <https://doi.org/10.1038/s41589-020-0559-0>.
- (23) Banks, A. M.; Whitfield, C. J.; Brown, S. R.; Fulton, D. A.; Goodchild, S. A.; Grant, C.; Love, J.; Lendrem, D. W.; Fieldsend, J. E.; Howard, T. P. Key Reaction Components Affect the Kinetics and Performance Robustness of Cell-Free Protein Synthesis Reactions. *Computational and Structural Biotechnology Journal* 2022, 20, 218–229. <https://doi.org/10.1016/j.csbj.2021.12.013>.
- (24) Gilman, J.; Walls, L.; Bandiera, L.; Menolascina, F. Statistical Design of Experiments for Synthetic Biology. *ACS Synth. Biol.* 2021, 10 (1), 1–18. <https://doi.org/10.1021/acssynbio.0c00385>.
- (25) Malci, K.; Walls, L. E.; Rios-Solis, L. Rational Design of CRISPR/Cas12a-RPA Based One-Pot COVID-19 Detection with Design of Experiments. *ACS Synth. Biol.* 2022, 11 (4), 1555–1567. <https://doi.org/10.1021/acssynbio.1c00617>.
- (26) Pardee, K.; Green, A. A.; Takahashi, M. K.; Braff, D.; Lambert, G.; Lee, J. W.; Ferrante, T.; Ma, D.; Donghia, N.; Fan, M.; Daringer, N. M.; Bosch, I.; Dudley, D. M.; O'Connor, D. H.; Gehrke, L.; Collins, J. J. Rapid, Low-Cost Detection of Zika Virus Using Programmable Biomolecular Components. *Cell* 2016, 165 (5), 1255–1266. <https://doi.org/10.1016/j.cell.2016.04.059>.
- (27) Blum, S. M.; Lee, M. S.; Mgboji, G. E.; Funk, V. L.; Beabout, K.; Harbaugh, S. V.; Roth, P. A.; Liem, A. T.; Miklos, A. E.; Emanuel, P. A.; Walper, S. A.; Chávez, J. L.; Lux, M. W. Impact of Porous Matrices and Concentration by Lyophilization on Cell-Free Expression. *ACS Synth. Biol.* 2021, 10 (5), 1116–1131. <https://doi.org/10.1021/acssynbio.0c00634>.
- (28) Lopreside, A.; Wan, X.; Michelini, E.; Roda, A.; Wang, B. Comprehensive Profiling of Diverse Genetic Reporters with Application to Whole-Cell and Cell-Free Biosensors. *Anal. Chem.* 2019, 91 (23), 15284–15292. <https://doi.org/10.1021/acs.analchem.9b04444>.
- (29) Siegal-Gaskins, D.; Tuza, Z. A.; Kim, J.; Noireaux, V.; Murray, R. M. Gene Circuit Performance Characterization and Resource Usage in a Cell-Free “Breadboard.” *ACS Synth. Biol.* 2014, 3 (6), 416–425. <https://doi.org/10.1021/sb400203p>.
- (30) Haeuser, C.; Goldbach, P.; Huwyler, J.; Friess, W.; Allmendinger, A. Impact of Dextran on Thermal Properties, Product Quality Attributes, and Monoclonal Antibody Stability in Freeze-Dried Formulations. *European Journal of Pharmaceutics and Biopharmaceutics* 2020, 147, 45–56. <https://doi.org/10.1016/j.ejpb.2019.12.010>.
- (31) Johnson, R. E.; Kirchhoff, C. F.; Gaud, H. T. Mannitol–Sucrose Mixtures—Versatile Formulations for Protein Lyophilization. *Journal of Pharmaceutical Sciences* 2002, 91 (4), 914–922. <https://doi.org/10.1002/jps.10094>.

- (32) Wilding, K. M.; Zhao, E. L.; Earl, C. C.; Bundy, B. C. Thermostable Lyoprotectant-Enhanced Cell-Free Protein Synthesis for on-Demand Endotoxin-Free Therapeutic Production. *New Biotechnology* 2019, 53, 73–80. <https://doi.org/10.1016/j.nbt.2019.07.004>.
- (33) Izutsu, K.; Yoshioka, S.; Terao, T. Stabilizing Effect of Amphiphilic Excipients on the Freeze-thawing and Freeze-drying of Lactate Dehydrogenase. *Biotech & Bioengineering* 1994, 43 (11), 1102–1107. <https://doi.org/10.1002/bit.260431114>.
- (34) Warfel, K. F.; Williams, A.; Wong, D. A.; Sobol, S. E.; Desai, P.; Li, J.; Chang, Y.-F.; DeLisa, M. P.; Karim, A. S.; Jewett, M. C. A Low-Cost, Thermostable, Cell-Free Protein Synthesis Platform for On-Demand Production of Conjugate Vaccines. *ACS Synth. Biol.* 2023, 12 (1), 95–107. <https://doi.org/10.1021/acssynbio.2c00392>.
- (35) Lu, Y. Textile-Embedded Cell-Free Biosensors. *Nat. Biomed. Eng* 2022, 6 (3), 225–226. <https://doi.org/10.1038/s41551-022-00869-3>.
- (36) Nguyen, P. Q.; Soenksen, L. R.; Donghia, N. M.; Angenent-Mari, N. M.; De Puig, H.; Huang, A.; Lee, R.; Slomovic, S.; Galbersanini, T.; Lansberry, G.; Sallum, H. M.; Zhao, E. M.; Niemi, J. B.; Collins, J. J. Wearable Materials with Embedded Synthetic Biology Sensors for Biomolecule Detection. *Nat Biotechnol* 2021, 39 (11), 1366–1374. <https://doi.org/10.1038/s41587-021-00950-3>.

531  
532  
533  
534  
535  
536  
537  
538  
539

## Supplemental Information

### High-Throughput Optimization of Paper-Based Cell-Free Biosensors

David C. Garcia<sup>1</sup>, John P. Davies<sup>1</sup>, Charles E. Davidson<sup>2</sup>, Daniel A. Phillips<sup>1</sup>, Aleksandr E. Miklos<sup>1</sup>, Matthew M. Lux<sup>1\*</sup>

<sup>1</sup>US Army DEVCOM Chemical Biological Center, Aberdeen Proving Ground, MD, USA

<sup>2</sup>Science and Technology Corporation, Belcamp, MD, USA



## 540 **Supplementary Results**

### 541 **Design of experiments**

542

#### 543 *Compressing data with Functional Principal Component analysis*

544

545 In order to fit the DOE models described above, the curves were first decomposed into  
546 Functional Principal Components (FPC). Results of the FPC decomposition of DOE for adding  
547 PANOx-SP components to baseline Cai are described in this section. After an initial FPC  
548 decomposition, we plotted the FPC1 scalars to identify any systematic issues (**Figure S7**). The  
549 experimental design is such that output should be randomly distributed across the samples, so  
550 any observed patterns indicate potential issues. Of the first 17 samples, 16 had minimal activity.  
551 We expect that this anomaly arose from a dispensing error by the acoustic liquid handler.  
552 Because the anomaly was systematic, we excluded samples 1-17 from further analysis. This  
553 anomaly further raises the question of other potential dispensing errors that do not result in an  
554 obvious systematic error. While we do not rule out this possibility, we note that DOE methods  
555 are generally robust to experimental errors.

556

557 After removing the outliers, we found that 94.8% of the variation could be explained by a single  
558 Eigenfunction (FPC1) representing a generic sigmoid shape (**Figure S8**). A second  
559 Eigenfunction (FPC2) explains an additional 4.85% of variation by dampening the slope of the  
560 response and introducing a positive slope to the plateau. Because FPC1 alone explains the  
561 data well, we used the FPC1 scalar as our fit metric.

562

563 An alternative choice to using FPC1 as the design objective would be to use the time until  
564  $\Delta E \geq 10$ . Since our goal is to create fast sensors, this alternative choice would be more direct;  
565 however, the use of FPC1 does indirectly select for response time by maximizing the linear  
566 scaling of FPC1 without discarding additional information about curve shape. To check what  
567 impacts the choice of a different objective function might have had, we re-ran the DOE analysis  
568 with time to  $\Delta E \geq 10$  as the objective. We found that the profile of median amount of each  
569 component added was similar across the top 10 predicted optimals, suggesting that the search  
570 space represented by each set of predicted optimals is likely similar (**Figure S9**). Since little  
571 difference was observed, we chose to proceed with FPC1 as our objective function because of  
572 our anticipated-but-unverified notion that capturing the full curve information can help mitigate  
573 the impact of outliers.

574

#### 575 *Descriptions of DOE models used*

576

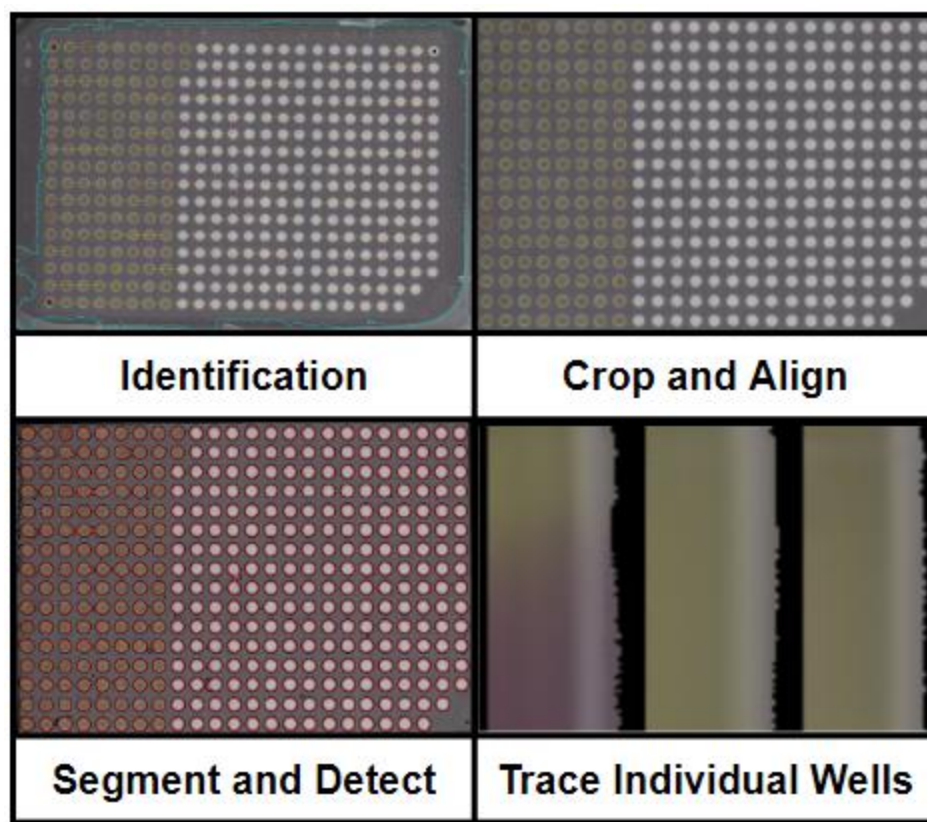
577 The initial design for this experiment was a screening design intended to identify whether  
578 components of the Cai formulation could be added to recover activity of baseline Cai reactions.  
579 A quadratic Mixture Amount design with 16 components and a single process factor, labeled  
580 "Total Volume", was used (**Supplementary Data Files**). The process factor allowed for variation  
581 in the total number of droplets dispensed across all components added to the base Cai reaction.  
582 Because the reactions are then lyophilized, we do not expect this process factor to play a  
583 significant role in the predictive model. A Quadratic starting model was used with a "KVC" cross.  
584 This design is I-Optimal and capable of fitting non-linear blending effects up to second order and  
585 interactions with the "Total Volume" factor up to 2-way. This design models the influences of the  
586 relative ratios of the 16 components as well as the "Total Volume". Despite identifying some  
587 combinations that yielded a response, the high number of non-responsive formulations resulted  
588 in an ability of the DOE model to fit the data using a backward (BiC) reduced statistical model.

589

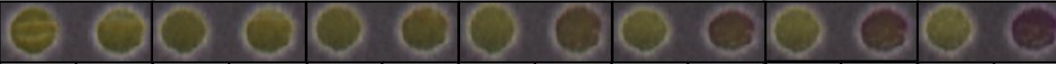
590 The second attempt mirrored the first except 14 components from the PANOx-SP formulations  
591 were added instead, as described in the main text. The detailed design is available in the  
592 **Supplementary Data Files**. The resulting data was adequate for fitting the DOE model. A  
593 backward (BiC) reduced statistical model was fit to the FPC1 data. The resulting model  
594 ( $R^2=0.6848$ ,  $p<0.0001$ ) had 34 terms including linear effects for the 14 reaction components and  
595 20 additional non-linear blending effects that were influential enough to be included in the  
596 model. These effects and their blending coefficients are detailed in **Table S7-8**. These effects  
597 are interpreted in the main text.

598  
599 The DOE for heat tolerance followed the same approach except 14 excipients were added to  
600 baseline PANOx-SP reactions. Details of the DOE is available in the **Supplementary Data**  
601 These effects and their blending coefficients are detailed in **Table S11-12**. These effects are  
602 again interpreted in the main text.

603  
604



605 **Figure S1:** Representative example of 384-well CFE paper ticket analysis software extracting color  
606 change information for individual wells.  
607



Time (min)	0	0	18	18	38	38	52	52	58	58	60	60	78.4	78.4
$\Delta E$	0.0	0.0	-0.7	0.1	-0.8	0.46	-0.7	4.2	-0.8	8.8	-0.71	10.6	-0.4	24.2

608

609

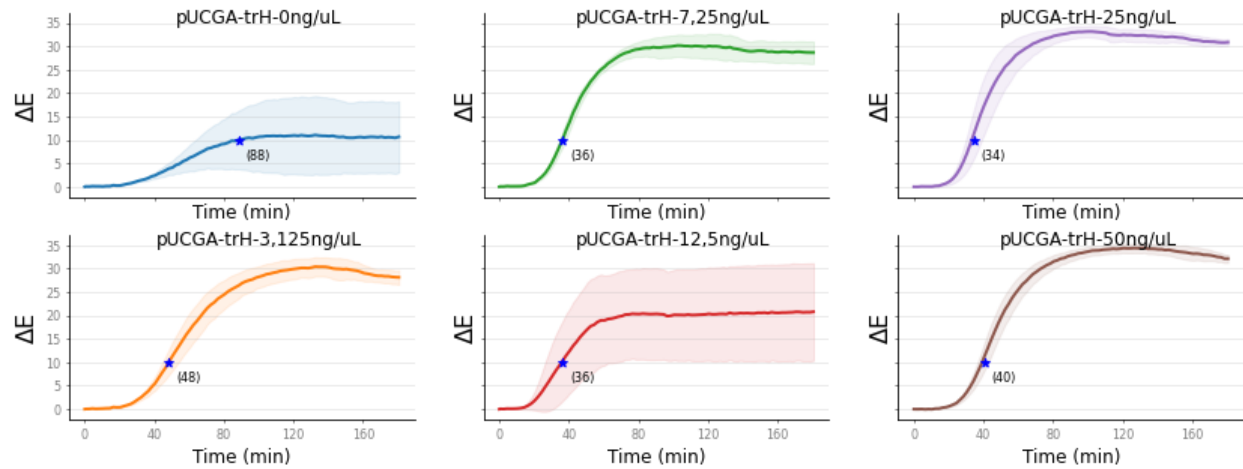
610

611

612

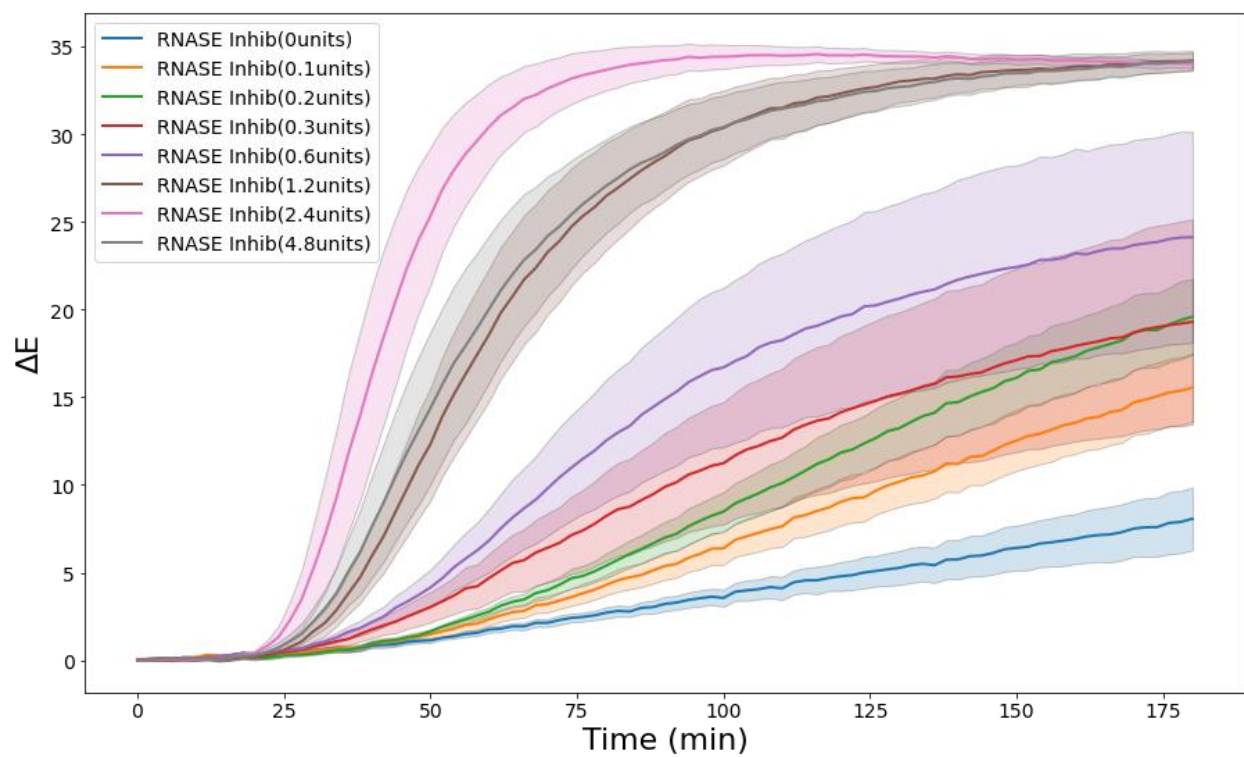
613

**Figure S2:** A representative image of the color change over time in a cell-free biosensor using a colorimetric reporter. Though a perceivable color change is seen earlier, we chose  $\Delta E \geq 10$  as a threshold at which the color change is obvious.



614  
615 **Figure S3:** A PANOx-SP CFPS reagent mix was prepared with the same amount of pUCGA-swH-LacZ  
616 plasmid directly added before lyophilization and activated by resuspending using various concentrations  
617 of the commensurate trH. The blue star indicates the point at which a  $\Delta E \geq 10$  was reached. Standard  
618 deviations shown as shadows on each trace were derived from quadruplicate reactions.

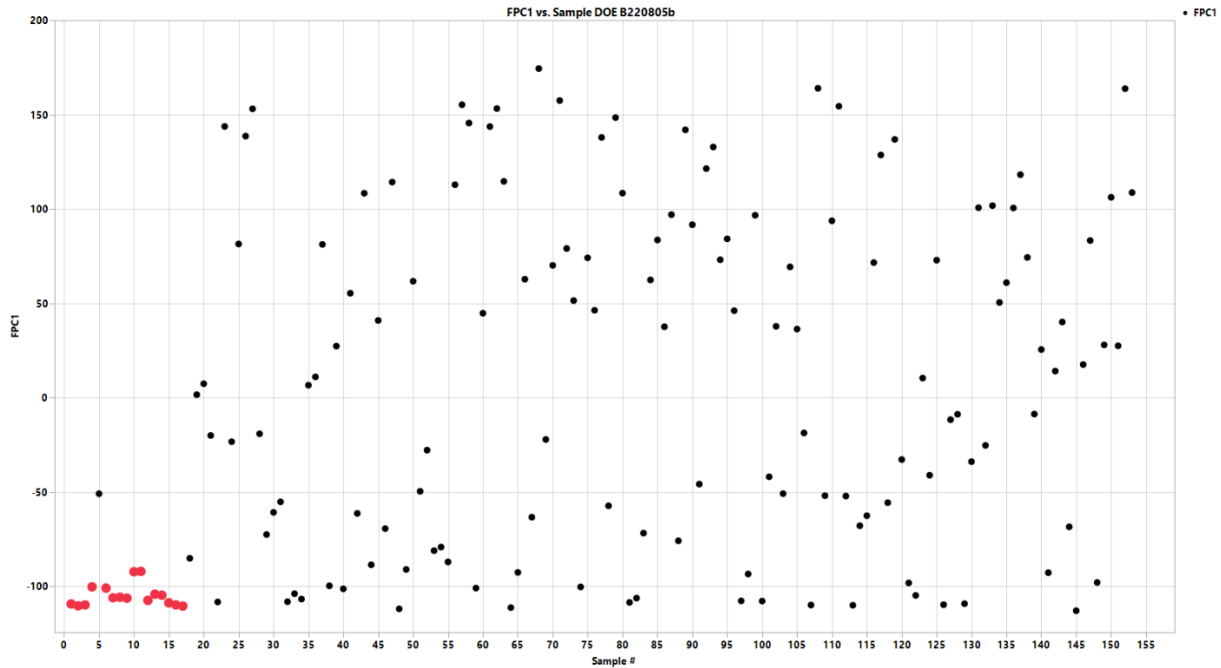
619



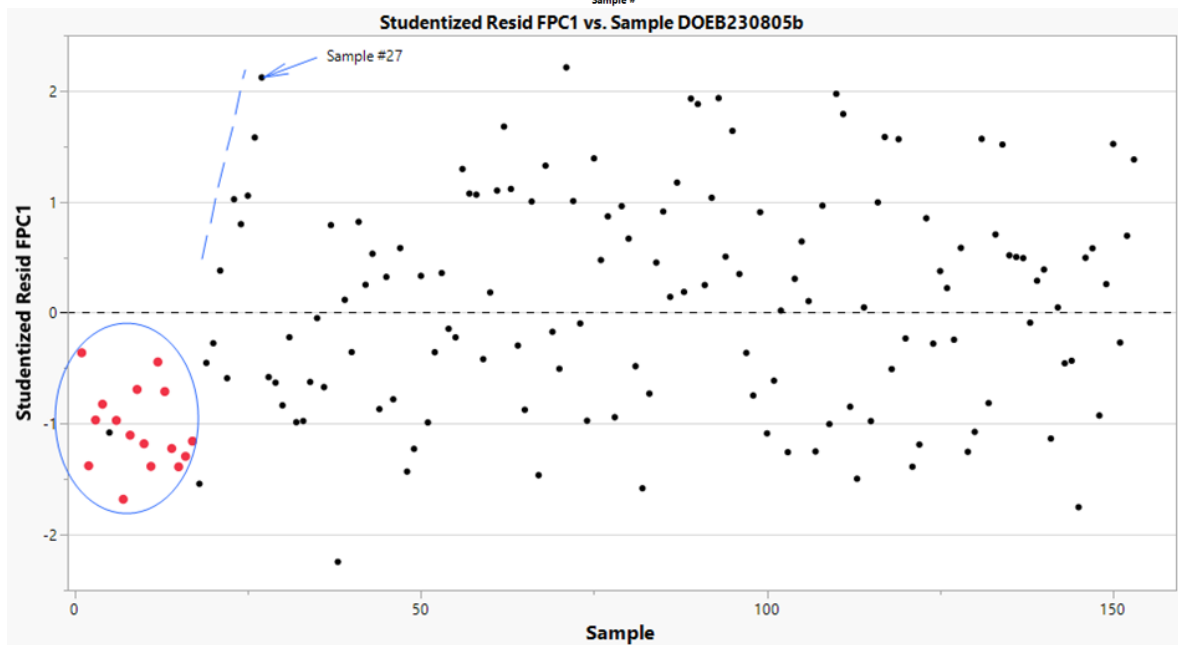
620

621 **Figure S4:** Effect of increasing amounts of RNase Inhibitor added to the reaction mixture.

622



623



624

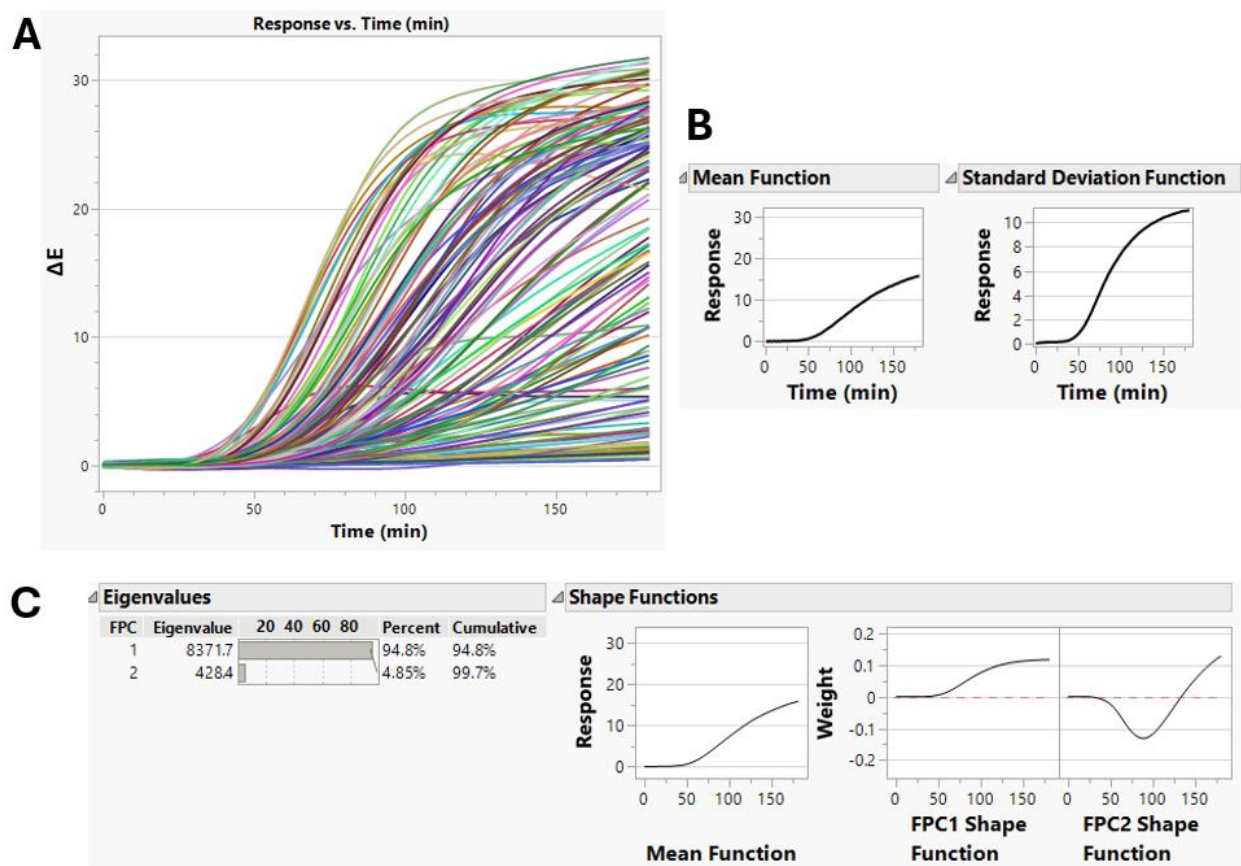
625

626

627

628

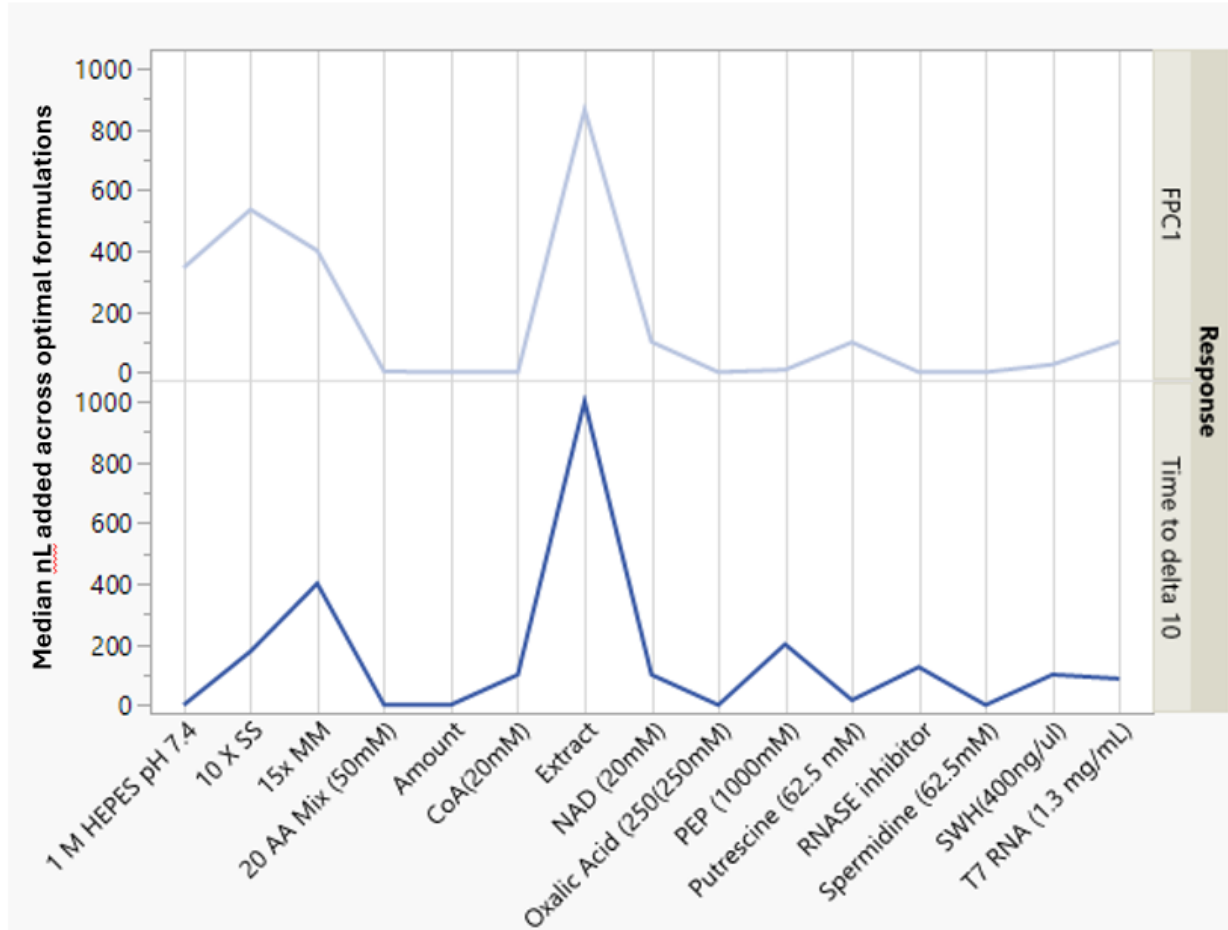
**Figure S5:** Extracted FPC1 values as a function of DOE number from PANOx-SP components added to baseline Cai. **(top)** Raw FPC1 values. **(bottom)** Studentized residuals. Red dots indicate region of apparent of unexpected systematic bias.



629  
630  
631  
632  
633  
634

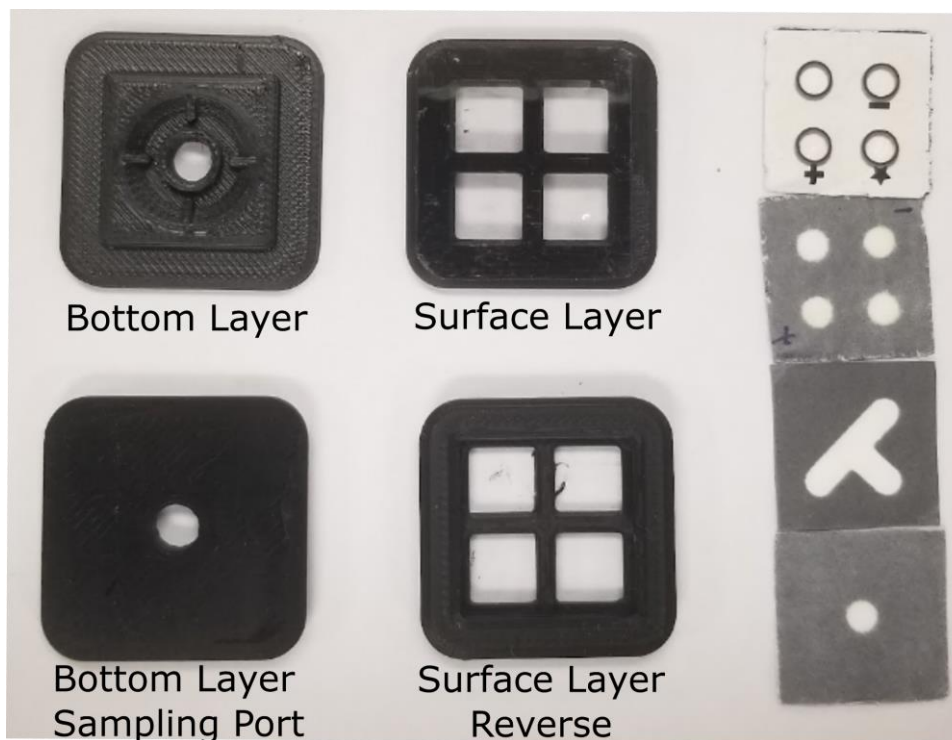
**Figure S6:** Functional Principal Component decomposition of curves resulting from DOE of adding PANOX-SP components to baseline Cai reactions. **(A)** Raw traces of  $\Delta E$  over time extracted from images. **(B)** Mean and standard deviation functions of the full data set after removal of outliers. **(C)** Results of FPC analysis.





635  
636  
637  
638

**Figure S7:** Median volumes of each component added in the predicted optimal formulations based on optimizing for FPC1 (**top**) or time to  $\Delta E \geq 10$  (**bottom**).



639  
640  
641  
642  
643

**Figure S8.** Fitted bottom and surface layers hold together the paper fluidics. Sample is added directly to the sampling port and visualized on the surface layer covered in transparent film.

644 **Table S1:** Cost comparison of CFE reactions using Cai and PANox-SP formulations. Media  
 645 calculations assume 300 mL per L, and 3 mL of lysate made per L of media.  
 646

	<b>Cai</b>	<b>PANox-SP</b>
<i>Media Components for Lysate</i>		
Tryptone	\$ 77.10	\$ 77.10
Yeast Extract	\$ 34.80	\$ 34.80
NaCl	\$ 3.41	\$ 3.41
Potassium phosphate, monobasic	\$ 10.75	\$ 10.75
Potassium phosphate, monobasic	\$ 10.26	\$ 10.26
DTT	\$ 87.41	\$ 87.41
<i>CFE Components</i>		
YNB	\$ -	\$ -
HEPES	\$ -	\$ 5.79
Tris	\$ -	\$ -
Potassium Phosphate	\$ 0.16	\$ -
ATP	\$ -	\$ 40.67
GTP	\$ -	\$ 302.40
CTP	\$ -	\$ 227.61
UTP	\$ -	\$ 469.13
AMP	\$ 6.52	\$ -
GMP	\$ 3.54	\$ -
CMP	\$ 17.57	\$ -
UMP	\$ 5.57	\$ -
Oxidized glutathione	\$ 5.69	\$ -
Tyrosine	\$ 0.12	\$ -
PEP	\$ -	\$2,142.72
NAD	\$ -	\$ 728.32
CoA	\$ -	\$ 681.80
Potassium Glutamate	\$ 16.01	\$ 10.78
Ammonium Glutamate	\$ -	\$ 0.62
Magnesium Glutamate	\$ 8.62	\$ 17.25
Sodium/Potassium Oxalate	\$ 0.05	\$ 0.05
Putrescine	\$ -	\$ 0.70
Spermidine	\$ 5.05	\$ 5.05
Alanine	\$ 0.11	\$ 0.11
Arginine	\$ 0.13	\$ 0.13
Asparagine	\$ 0.20	\$ 0.20
Aspartic acid	\$ 0.03	\$ 0.03
Cysteine	\$ 0.19	\$ 0.19
Glutamic acid	\$ 0.02	\$ 0.02
Glutamine	\$ 0.16	\$ 0.16
Glycine	\$ 0.02	\$ 0.02

Histidine	\$ 0.17	\$ 0.17
Isoleucine	\$ 0.25	\$ 0.25
Leucine	\$ 0.15	\$ 0.15
Lysine	\$ 0.99	\$ 0.99
Methionine	\$ 0.11	\$ 0.11
Phenylalanine	\$ 0.19	\$ 0.19
Proline	\$ 0.13	\$ 0.13
Serine	\$ 0.15	\$ 0.15
Threonine	\$ 0.25	\$ 0.25
Tryptophan	\$ 0.31	\$ 0.31
Tyrosine	\$ 0.26	\$ 0.26
Valine	\$ 0.12	\$ 0.12
Folic Acid	\$ -	\$ 89.25
E. coli tRNA	\$ -	\$ 246.58
DNA Template	\$ 92.03	\$ 92.03
T7 RNA polymerase	\$ 56.40	\$ 282.00
<b>Total:</b>	<b>\$444.97</b>	<b>\$5,570.37</b>

647

648 **Table S2:** Energy mixture components for PANOx-SP base reactions.

649

<b>Component</b>	<b>PANOx-SP Final Concentration</b>
Magnesium	12 mM
Potassium glutamate	130 mM
Ammonium glutamate	10 mM
Magnesium acetate	3.7 mM
Potassium acetate	6.2 mM
Tris acetate	5.67 mM (pH 8.2)
HEPES	7.5 mM (pH 7.4)
ATP	1.2 mM
GTP	0.85 mM
CTP	0.85 mM
UTP	0.85 mM
Folic acid	0.072 mM
tRNA	170.6 µg/mL
Alanine	2 mM
Arginine	2 mM
Histidine	2 mM

Lysine (monoHCl)	2 mM
Aspartic acid	2 mM
Glutamic acid	2 mM
Isoleucine	2 mM
Leucine	2 mM
Methionine	2 mM
Phenylalanine	2 mM
Tryptophan	2 mM
Tyrosine	2 mM
Valine	2 mM
Serine	2 mM
Threonine	2 mM
Asparagine	2 mM
Glutamine	2 mM
Cysteine	2 mM
Glycine	2 mM
Proline	2 mM
PEP	33 mM
NAD	0.33 mM
CoA	0.27 mM
Spermidine	1.5 mM
Putrescine	2 mM
Oxalic acid	4 mM
<hr/>	
T7 RNA polymerase	100 $\mu$ g/mL
Plasmid DNA	6.4 nM
RNase Inhibitor	1.2 U/ $\mu$ L
Cell extract	30% v/v
DTT	0.5 mM

650

651

652

653

654

655

656

657

658

659

**Table S3.** Energy mixture components for Cai base reactions.

660

<b>Component</b>	<b>Concentration</b>
AMP	1.2 mM
UMP	0.86 mM
CMP	0.86 mM
GMP	0.86 mM
T7 RNA Polymerase	0.02 mg/mL
Magnesium Glutamate	8 mM
Potassium Glutamate	260 mM
Potassium Oxalate	4 mM
Potassium Phosphate pH 7.0	15 mM
Spermidine	1.5 mM
Oxidized Glutathione	2 mM
Alanine	2 mM
Arginine	2 mM
Histidine	2 mM
Lysine (monoHCl)	2 mM
Aspartic acid	2 mM
Glutamic acid	2 mM
Isoleucine	2 mM
Leucine	2 mM
Methionine	2 mM
Phenylalanine	2 mM
Tryptophan	1 mM
Tyrosine	2 mM
Valine	2 mM
Serine	2 mM
Threonine	2 mM
Asparagine	2 mM
Glutamine	2 mM

Cysteine	2 mM
Glycine	2 mM
Proline	2 mM
Cell extract	30% v/v
RNase Inhibitor	1.2 U/ $\mu$ L

661  
662  
663

**Table S4** Working solutions used in energy mixture components for PANOx-SP reagent additives.

Reagent	Concentration
Salt Solution (SS)	10X
HEPES	1 M
Cell-Free Master Mix (MM)	15X
AA Mix	50 mM
PEP	1 M
NAD	20 mM
CoA	20 mM
Oxalic Acid	250 mM
Putrescine	62.5 mM
Spermidine	62.5 mM
T7 RNAP	1.3 mg/mL
RNASE inhibitor Murine Extract	4 units/ $\mu$ L ~30 mg/mL
CPRG	-
DNA (each plasmid)	400 ng/ $\mu$ l

664  
665

**Table S5:** Working solutions used in energy mixture components for Cai reagent additives.

666  
667

Reagent	Concentration
L-Glutamic acid hemimagnesium salt tetrahydrate	40 mM
L-Glutamic acid monopotassium salt monohydrate	1300 mM
AMP	25 mM
GMP	25 mM
UMP	25 mM
CMP	25 mM
Oxalic Acid	150 mM
L-Glutathione oxidized	50 mM
Spermidine	125 mM
Potassium phosphate ( $K_2HPO_4$ )	307.5 mM

Potassium phosphate (KH <sub>2</sub> PO <sub>4</sub> )	192.5 mM
Amino Acids (19)	25 mM
Tyrosine	25 mM
T7 RNAP	1.3 mg/mL
RNASE inhibitor Murine	-
Lysate	~30 mg/mL
CPRG	-
DNA (each plasmid)	400 ng/μl

668

669 **Table S6:** Excipients tested for heat tolerance.

670

Excipient	Concentration	Role	Reference
Dextran 70	50 mg/mL	Cryoprotectant	<i>Hagen et al. (1997)</i>
PEG8K	5%	Lyoprotectant	<i>Manning et al. (2010)</i>
Maltose	50 mM	Cryoprotectant	<i>Chirife et al. (2000)</i>
H <sub>2</sub> KPO <sub>4</sub>	50 mM	Buffering agent	<i>Pikal-Cleland et al. (2000)</i>
Ficoll	50 mg/mL	Cryoprotectant	<i>Wang et al. (2006)</i>
Maltodextrin	50 mM	Bulking agent	<i>Patel and Pikal (1996)</i>
Raffinose	50 mM	Cryoprotectant	<i>Wang et al. (2006)</i>
Lactose	50 mM	Cryoprotectant	<i>Wang et al. (2006)</i>
Rhamnose	50 mM	Cryoprotectant	<i>Chirife et al. (2000)</i>
Mannitol	50 mM	Cryoprotectant	<i>Wang et al. (2006)</i>
Sucrose	50 mM	Cryoprotectant	<i>Wang et al. (2006)</i>
Malitol	50 mM	Cryoprotectant	<i>Wang et al. (2006)</i>
Sorbitol	50 mM	Cryoprotectant	<i>Chirife et al. (2000)</i>
TMAO	50 mM	Stabilizer/Protectant	<i>Wüstner and Solanko (2015)</i>

671

672 **Table S7:** Linear blending coefficients from the DOE model of PANOX-SP components added to baseline

673 Cai. Positive coefficients indicate an increase in FPC1 as the proportion of the component changes.

674

Linear Blending Coefficient	Name
133.6	1 M HEPES pH 7.4
124.7	Oxalic Acid (250(250mM)
117.1	SWH(400ng/μl)
88.7	T7 RNA (1.3 mg/mL)
70.1	CoA(20mM)
61.2	15x MM
44.6	Putrescine (62.5 mM)
23.3	NAD (20mM)
10.9	Extract
-2.7	Spermidine (62.5mM)
-21.8	10 X SS
-23.9	20 AA Mix (50mM)



---

-115.2	RNASE inhibitor
-151.5	PEP (1000mM)

---

675  
676

677 **Table S8:** Non-linear blending coefficients from the DOE model of PANOx-SP components added to  
678 baseline Cai. Positive coefficients indicate an increase in FPC1 as the proportion of the component  
679 changes.  
680

<b>Non-linear Blending Coefficient</b>	<b>Component Names</b>
1,654.40	Spermidine (62.5mM)*RNASE inhibitor
1,173.80	CoA(20mM)*RNASE inhibitor
1,027.40	PEP (1000mM)*RNASE inhibitor
901.2	20 AA Mix (50mM)*Spermidine (62.5mM)
522.3	10 X SS*SWH(400ng/μl)
330.2	PEP (1000mM) * Extract
242	10 X SS*PEP (1000mM)
17.9	PEP (1000mM) * amount (total added)
6.7	Extract *amount (total added)
-45.1	SWH(400ng/μl)*amount (total added)
-72.8	Putrescine (62.5 mM) * amount (total added)
-196.2	1 M HEPES pH 7.4*Extract
-383	1 M HEPES pH 7.4 *PEP (1000mM)
-628.6	15x MM *CoA(20mM)
-967.3	1 M HEPES pH 7.4*Spermidine (62.5mM)
-1,361.90	15x MM*Oxalic Acid (250(250mM)
-1,541.70	CoA(20mM)*Oxalic Acid (250(250mM)
-1,565.00	1 M HEPES pH 7.4 * SWH(400ng/μl)
-2,299.30	Putrescine (62.5 mM) * SWH(400ng/μl)
-2,708.30	Spermidine (62.5mM)* T7 RNA (1.3 mg/mL)

681  
682

683 **Table S9:** Results of independent t-tests performed to compare the PANOx-SP controls against each  
684 experimental dataset when  $\Delta E \geq 10$  for the optimized Cai formulations. The p-values assess the statistical  
685 significance of these differences using  $n=4$  samples.  
686

<b>Comparison</b>	<b>p-value</b>
Cai+Opt1	0.415247
Cai+Opt2	0.650334
Cai+Opt3	0.256598
Cai+Opt4	0.816178
Cai+Opt5	0.871965
Cai+Opt6	0.96559
Cai+Opt7	0.252361
Cai+Opt8	0.407565
Cai+Opt9	0.735271

687  
688

689 **Table S10:** Cost breakdown of Cai optimized formulations. Costs are given per 1  $\mu$ L reaction.  
690

Index	Cai-Opt Costs	Baseline Cai Cost	Total Cost per Reaction
1	\$ 1.95876	\$ 0.00044	\$ 1.95920
2	\$ 0.00129	\$ 0.00044	\$ 0.00173
3	\$ 0.00133	\$ 0.00044	\$ 0.00177
4	\$ 1.96275	\$ 0.00044	\$ 1.96320
5	\$ 0.00132	\$ 0.00044	\$ 0.00177
6	\$ 0.00131	\$ 0.00044	\$ 0.00176
7	\$ 0.49299	\$ 0.00044	\$ 0.49343
8	\$ 1.96420	\$ 0.00044	\$ 1.96465
9	\$ 0.00141	\$ 0.00044	\$ 0.00186
10	\$ 1.95528	\$ 0.00044	\$ 1.95573
11	\$ 0.00021	\$ 0.00044	\$ 0.00065
12	\$ 0.49558	\$ 0.00044	\$ 0.49603
13	\$ 0.49721	\$ 0.00044	\$ 0.49766
14	\$ 0.00022	\$ 0.00044	\$ 0.00067
15	\$ 1.95924	\$ 0.00044	\$ 1.95968
16	\$ 0.00259	\$ 0.00044	\$ 0.00303
17	\$ 1.95974	\$ 0.00044	\$ 1.96018
18	\$ 0.00255	\$ 0.00044	\$ 0.00300
19	\$ 0.49694	\$ 0.00044	\$ 0.49738
20	\$ 0.50248	\$ 0.00044	\$ 0.50293
21	\$ 0.49139	\$ 0.00044	\$ 0.49184
22	\$ 1.96049	\$ 0.00044	\$ 1.96094
23	\$ 1.95581	\$ 0.00044	\$ 1.95625
24	\$ 1.96259	\$ 0.00044	\$ 1.96304
25	\$ 1.47543	\$ 0.00044	\$ 1.47588
26	\$ 0.00316	\$ 0.00044	\$ 0.00361

27	\$ 1.96094	\$ 0.00044	\$ 1.96138
28	\$ 0.00442	\$ 0.00044	\$ 0.00487
29	\$ 0.97770	\$ 0.00044	\$ 0.97814
30	\$ 1.96160	\$ 0.00044	\$ 1.96204

691

692 **Table S11:** Linear blending coefficients from the DOE model of heat tolerance excipients added to  
693 baseline PANOx-SP. Positive coefficients indicate an increase in FPC1 as the proportion of the  
694 component changes.  
695

<b>Linear Blending Coefficient</b>	<b>Component Name</b>
258.4	Raffinose 50mM
170.5	Maltose 50mM
136.9	Ficoll 50mM
132.4	TMAO 50mM
131.2	Maltodextrin 50mM
72.3	Sorbitol 50mM
33.5	H2KPO4
18.8	Dextran 70 50 mM
-62.6	Sucrose 50mM
-107.8	Mannitol 50mM
-126.1	Lactose 50mM
-135.7	Malitol 50mM
-248.4	PEG5%
-290.8	Rhamnose 50mM

696  
697

698 **Table S12:** Non-linear blending coefficients from the DOE model of heat tolerance excipients added to  
699 baseline PANOx-SP. Positive coefficients indicate an increase in FPC1 as the proportion of the  
700 component changes.  
701

<b>Non-linear Blending Coefficient</b>	<b>Component Names</b>
1580.7	Dextran 70 50 mM*Mannitol 50mM
1453.4	PEG5%*Rhamnose 50mM
1203.2	Sucrose 50mM*Malitol 50mM
1158.8	Lactose 50mM*Rhamnose 50mM
1136.7	Maltodextrin 50mM*Sucrose 50mM
1119.7	H2KPO4*Ficoll 50mM
996.2	Mannitol 50mM*Malitol 50mM
751.6	H2KPO4*Raffinose 50mM
669.2	Ficoll 50mM*Rhamnose 50mM
389.6	Maltose 50mM*Malitol 50mM
-443.1	Dextran 70 50 mM*Malitol 50mM
-659.5	PEG5%*Sucrose 50mM
-729.5	Dextran 70 50 mM*Ficoll 50mM
-735.3	Maltose 50mM*Ficoll 50mM
-750.8	Maltose 50mM*H2KPO4
-853.5	Maltose 50mM*Maltodextrin 50mM
-1038.9	Raffinose 50mM*Sorbitol 50mM
-1100.2	Maltodextrin 50mM*TMAO 50mM
-1120.1	Maltose 50mM*TMAO 50mM
-1423.1	Ficoll 50mM*Rhamnose 50mM

702  
703

704 **Table S13.** Results of independent t-tests performed to compare the point where of  $\Delta E \geq 10$  for PANOx-SP  
705 dataset from the Cai optimization experiment against the heat optimized formulations (Heat-Opt1 through  
706 Heat-Opt14). The p-values assess the statistical significance of these differences using n=4 samples.  
707

<b>Comparison</b>	<b>p-value</b>
PANOx-SP vs Heat-Opt1	0.94
PANOx -SP vs Heat-Opt2	0.99
PANOx -SP vs Heat-Opt3	0.96
PANOx -SP vs Heat-Opt4	0.98
PANOx -SP vs Heat-Opt5	0.83
PANOx -SP vs Heat-Opt6	0.96
PANOx -SP vs Heat-Opt7	0.99
PANOx -SP vs Heat-Opt8	0.97
PANOx -SP vs Heat-Opt9	0.79
PANOx -SP vs Heat-Opt10	0.97
PANOx -SP vs Heat-Opt11	0.97
PANOx -SP vs Heat-Opt12	0.97
PANOx -SP vs Heat-Opt13	0.92
PANOx -SP vs Heat-Opt14	0.87

708  
709



710  
711